



Final Report

Project title: Hydrogen fuel production from seawater using dual-doped BiVO₄ photocatalysts

by

Dr. Ratiporn Munprom

May 2020

Final Report

Project title: Hydrogen fuel production from seawater using dual-doped BiVO₄ photocatalysts

Principal investigator

Dr. Ratiporn Munprom

Department of Materials Engineering, Kasetsart University

Mentor

Prof.Dr. Metta Chareonpanich

Department of Chemical Engineerin, Kasetsart University

Project Granted by the Thailand Research Fund and Kasetsart University

บทคัดย่อ

รหัสโครงการ: MRG6180134

ชื่อโครงการ: โครงการการผลิตเชื้อเพลิงไฮโดรเจนจากน้ำทะเลโดยใช้ตัวเร่งปฏิกิริยาเชิงแสง BiVO₄ ที่เจือด้วยสารเจือสอง ชนิด

ชื่อหักวิจัย และสถาบัน: ดร.รติพร มั่นพรหม ภาควิชาวิศวกรรมวัสดุ คณะวิศวกรรมศาสตร์ มหาวิทยาลัยเกษตรศาสตร์

อีเมล์: fengrtpm@ku.ac.th

ระยะเวลาโครงการ: 2 ปี

บทคัดย่อ:

จากวิกฤตพลังงาน ทำให้ความต้องการในการใช้พลังงานทดแทนและเป็นพลังงานสะอาดไม่ก่อให้เกิดก๊าซเรือนกระจกสูงขึ้น ดังนั้น เทคโนโลยีการแยกน้ำเป็นไฮโดรเจนด้วยตัวเร่งปฏิกิริยาเชิงแสง ถือเป็นเทคโนโลยีหนึ่งที่สามารถผลิตพลังงานสะอาดได้ โดย ตัวเร่งปฏิกิริยาเชิงแสงดูดกลืนพลังงานแสงอาทิตย์และเปลี่ยนน้ำให้เป็นไฮโดรเจน สารกึ่งตัวนำชนิดหนึ่งที่ได้รับความสนใจในเทคโนโลยีนี้ คือ บิธมัสวานาเดต เนื่องจากวัสดุชนิดนี้สามารถดูดกลืนแสงอาทิตย์ได้ดี มี ความเสถียรและไม่เป็นพิษต่อสิ่งแวดล้อม ดังนั้น จึงมีความพยายามในการพัฒนาประสิทธิภาพของตัวเร่งปฏิกิริยาเชิงแสงนี้ โครงการวิจัยนี้ ได้นำเสนอวิธีการในการปรับปรุงประสิทธิภาพของตัวเร่งปฏิกิริยาเชิงแสง โดยการศึกษาผลของการเจือที่มีต่อสมบัติ และประสิทธิภาพของสารบิสมัธวานาเดตที่มีองค์ประกอบทางเคมีไม่สมดุล กล่าวคือ มีองค์ประกอบของบิสมัธหรือวานาเดียมขาด ซึ่งผลการศึกษาพบว่า การเจือที่ผลต่อการเกิดเฟสของบิสมัธวานาเดต รวมถึงสารเจือสามารถแทนที่อะตอมวานาเดียมในโครงสร้าง ได้ง่ายกล่าวอะตอมบิสมัธ นอกจากนี้ หากมีการเจือสารในปริมาณน้อย (ไม่เกิน 5 เปอร์เซ็นต์โดยโมล) โครงสร้างของบิสมัธรานา เดตที่ได้ไม่แตกต่าง แต่ชนิดของสารเจือมีผลทำให้ลักษณะสัณฐานวิทยาแตกต่างกัน กล่าวคือ สารเจือทำให้เกิดนิวเคลียสในการเกิด ผลึกได้ง่ายขึ้นทำให้ผงที่สังเคราะห์ได้มีขนาดอนุภาคเล็กลง

นอกจากนี้ประสิทธิภาพการเร่งปฏิริยาเชิงแสงของสารที่มีการเจือสารสองชนิดขึ้นอยู่กับชนิดของสารเจือ โดยบิสมัธวานาเดทที่ เจือดีบุกและโมลิบดินัมมีประสิทธิภาพในการเร่งปฏิกิริยาเชิงแสงดีกว่าสารเจือชนิดอื่นที่ศึกษา สาเหตุที่เป็นเช่นนั้น อาจ เนื่องมาจากขนาดอะตอมของดีบุกมีขนาดเล็กกว่าอะตอมอื่นๆ ที่ศึกษา ทำให้เมื่อเกิดการแทนที่ภายในโครงสร้างแล้ว โครงสร้าง เกิดการบิดเบี้ยวมากกว่าสารเจือชนิดอื่นทำให้โครงสร้างไม่สมมาตรและเกิดการเหนี่ยวนำโพลาไรเซชันภายในโครงสร้างที่ช่วยแยก อิเล็กตรอนกับโฮล ทำให้ประสิทธิภาพการเร่งปฏิกิริยาเชิงแสงดีขึ้น

สำหรับการศึกษาการพัฒนาโครงสร้างแบบวิวิธพันธ์นั้น พบว่าโครงสร้างแบบวิวิธพันธ์แสดงสมรรถภาพในการสร้างก๊าซ ไฮโดรเจนจากน้ำสูงกว่าโครงสร้างบิสมัธวานาเดตชั้นเดียว ประสิทธิภาพที่ดีขึ้นนี้อาจเนื่องมาจากโครงสร้างแบบวิวิธพันธ์ทำให้เกิด ความต่างศักย์ภายในที่รอยต่อของชั้นฟิล์มส่งผลให้เกิดการแยกอิเล็กตรอน-โฮลที่ดีกว่า ดังนั้น ผลการวิจัยนี้จึงแสดงแนวทางในการ ปรับปรุงประสิทธิภาพของตัวเร่งปฏิกิริยาทางแสงให้ดีขึ้นได้

คำหลัก (จำนวน 3-5 คำ): ตัวเร่งปฏิกิริยาเชิงแสง; บิสมัธวานาเดต; การเจือสองชนิด; การผลิตไฮโดรเจนจากน้ำ

Abstract

Project Code: MRG6180134

Project Title: Hydrogen fuel production from seawater using dual-doped BiVO₄

photocatalysts

Investigator : Dr. Ratiporn Munprom

Materials Engineering Department, Faculty of Engineering,

Kasetsart University

E-mail Address: fengrtpm@ku.ac.th

Project Period: 2 years

Abstract:

Due to the energy crisis, the world needs alternative energy resources that can lead to energy sustainability. Photocatalytic water splitting is one of alternative technologies for cleaner energy generation where solar energy is converted to chemical energy in the form of hydrogen fuel. One of promising photocatalysts that allures researchers is BiVO₄. This material is visible-light responsive, and it has shown high photocatalytic activity for water oxidation. Due to its potential, many researchers are attempting to improve its performance.

In this study, some strategies to improve efficiencies were proposed. An insight of the effect of dopant on properties of non-stoichiometric BiVO₄ compounds was obtained. The results reveal that doping in different non-stoichiometric environment, namely Bi-deficit and V-deficit causes different phase formation. In addition, dopants are more likely to substitute on V site than Bi site. In other words, the substitution of W on Bi site is less thermodynamically favourable. Plus, our strategy of dual doping can lead to modify the band structure of BiVO₄ resulting in improved photocatalytic activity. Dual-doping could induce a strain in a local structure leading to an internal polarization which could improve the efficiencies. Moreover, structure modification by heterostructure shows a promising performance because the heterostructure can enhance a charge separation. All results presented in the study provide an insight of how doping alters a structure which is a useful information for photocatalytic performance enhancement.

Keywords (3-5 words): photocatalyst; BiVO₄; hydrogen production; dual-doping

Table of Content

	Page
1. Abstract	1
2. Executive summary	2
3. Literature review	5
4. Objectives	10
5. Methodology	11
6. Results and Discussion	18
6.1 Study 1: The effect of doping on properties of	
non-stoichiometric BiVO ₄ compounds	18
6.2 Study 2: The effect of dual-doping on properties of	
BiVO ₄ related compounds	25
6.3 Study 3: The effect of heterostructure on BiVO ₄	
water splitting performance	35
7. Conclusions	42
8. Output	48
Appendix	49

Hydrogen fuel production from seawater using dual-doped BiVO₄ photocatalysts

1. Abstract

Due to the energy crisis, the world needs alternative energy resources that can lead to energy sustainability. Photocatalytic water splitting is one of alternative technologies for cleaner energy generation where solar energy is converted to chemical energy in the form of hydrogen fuel. One of promising photocatalysts that allures researchers is BiVO₄. This material is visible-light responsive, and it has shown high photocatalytic activity for water oxidation. Due to its potential, many researchers are attempting to improve its performance.

In this study, some strategies to improve efficiencies were proposed. An insight of the effect of dopant on properties of non-stoichiometric BiVO₄ compounds was obtained. The results reveal that doping in different non-stoichiometric environment, namely Bi-deficit and V-deficit causes different phase formation. In addition, dopants are more likely to substitute on V site than Bi site. In other words, the substitution of W on Bi site is less thermodynamically favourable.

Plus, our strategy of dual doping can lead to modify the band structure of BiVO₄ resulting in improved photocatalytic activity. Dualdoping could induce a strain in a local structure leading to an internal polarization which could improve the efficiencies. Moreover, structure modification by heterostructure shows a promising performance because the heterostructure can enhance a charge separation. All results presented in the study provide an insight of how doping alters a structure which is a useful information for photocatalytic performance enhancement.

2. Executive summary

An energy insufficiency is one of the global issues that may be encountered in the future. With the rapid development of industrialization and an increase in population driving to expansion in energy needs, this problem becomes more severe and it may come sooner than expected. Therefore, it is necessary to find alternative energy sources to substitute the current use of limited fossil fuels. The requirements of alternative energy that should be considered are cleanliness, affordability, harvesting/conversion efficiency, and sustainability.

Photocatalytic water splitting is one of attractive technologies for clean energy supply. In this study, some strategies to improve efficiencies of photocatalysts were proposed. Bismuth vanadate was chosen as a candidate for this study because it shows potential for high performance due to its visible-light absorbing ability, stability and non-toxicity. Firstly, to have an insight of how doping influences the structure and performance of BiVO₄, doping in non-stoichiometric BiVO₄, namely Bideficit and V-deficit. The result reveals that it is more likely that doping atoms substitute V site easier than Bi site. Secondly, BiVO₄ was modified by dual-doping on Bi and V sites, specifically various doping elements (In, Sn and Y) on Bi site and Mo on V site. The results show that with a small concentration of dopants (not exceed 5%), all synthesized compounds possessed a monoclinic sheelite structure. Even though the doping elements do not affect the phase formation, the morphologies of powder were altered. Doped compounds have higher surface area. This is possibly because dopants stimulate a nucleation resulting in smaller particle formation. For photocatalytic performance, it was found that Sn doped sample exhibited a higher performance. This could be attributed to a higher induced polarization caused by a larger mismatch between sizes

of Sn²⁺ and Bi³⁺ compared with the others. Lastly, the structure was modified to a heterostructure. This structure could improve a charge separation resulting in enhanced performance. As a result, a heterostructure demonstrated a significantly higher photocurrent compared with a single BiVO₄ layer. This implies that heterostructure modification would be a promising strategy to improve the performance.

Introduction to Research

Clean and renewable energy is one of the focal research topics in many countries due to the energy crisis. In particular to Thailand, for example, the ministry of energy stated that "In 2015, energy production in Thailand decreased, resulting in more imports to meet domestic demand" [1]. This situation indicates that, with the relentless increase in the world's energy consumption combined with depleting fossil fuel resources, demands for sustainable sources of energy increase. In relation to the energy economy, it is considered ideal to be able to produce energy from the most abundant natural resource on earth, such as water.

Photocatalytic water splitting, first discovered by Fujishima and Honda [2], has long been regarded as an alternative technology for solar fuel production. Exploring an efficient system for solar hydrogen production is both economically relevant, and scientifically appealing. Dispersed in water, a photocatalyst absorbs light, and, in return, produces gaseous O₂ and chemical fuel of H₂. To turn water into hydrogen fuel, an assistance of a photocatalyst is required. Over the past three decades, metal oxides have been studied deeply as a photocatalyst for water photolysis. They are well suited to converse photon into chemical energy in aqueous solution. However, to date, almost all oxide materials fall short due to their inadequacy in terms of suitable band gap energy for visible light absorption, appropriate band positions, chemical phase

stability, and an efficient spatial charge separation to avoid electron-hole recombination [7–9]. Achieving in developing metal oxides which overcome many of these problems have long been a challenge in the scientific community. Recently, a promising oxide of bismuth vanadate (BiVO₄) has emerged. Specifically, a number of investigations on a BiVO₄ photocatalyst has shown a potential to overcome the all above challenges [8, 10].

To fully utilize BiVO₄, the issue of its electronic band structure needs to also be addressed. Monoclinic BiVO₄ is well documented to have a suitable band gap for absorbing visible light. To improve its performance, band edge engineering by simultaneously doping on both Bi and V sites of BiVO₄ has just been recently suggested [11].

This research intends to modify the band edge positions of BiVO₄ by dual- doping and the structure aimed of performance improvement. The potential dopants for this study are tin (Sn), indium (In), and yttrium (Y) on Bi site and molybdenum (Mo) on V site. Hence, in order to understand the mechanism, the chemical and physical properties of modified BiVO₄ compounds are examined. Moreover, the photocatalytic performance of dual-doped BiVO₄ are investigated. In addition, the dopant effect is discussed and potentially gives an insight of the mechanism of band edge engineering. Plus, it provides options of dopants for improving photocatalytic performance by dual doping. In addition, the performance improvement by heterostructure is demonstrated and discussed in detail.

3. Literature review

3.1 Water splitting mechanism and requirement

Photocatalytic water splitting is an alternative technology for clean energy production. Specifically, clean hydrogen fuel is produced as a product of the process. The water splitting process involve three main steps (Figure 1) as follows [12, 13].

- (i) *Absorption*: a photocatalyst absorbs photon having energy greater than its band gap. This step results in photogenerated charge carriers, namely electrons and holes.
- (ii) Charge separation: the electron-hole pairs are separated and travel to the photocatalyst's surfaces for the reactions.Otherwise, the electrons and holes can be combined resulting in a reduction of efficiency.
- (iii) H_2 and O_2 evolution: the electrons and holes travel to the surface to participate in a reduction and an oxidation reaction, respectively. The reactions for H_2 and O_2 evolution are:

 H_2 evolution: $2H^+ + 2e^- \rightarrow H_2(gas)$

 O_2 evolution: $2h^+ + H_2O$ (liquid) $\rightarrow 1/2 O_2(gas) + 2H^+$

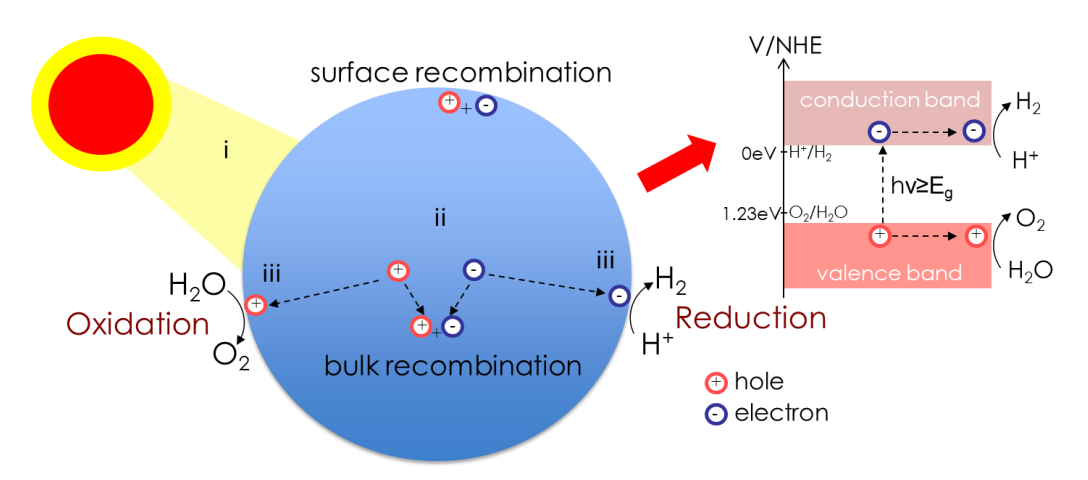


Figure 1. Mechanism of photocatalytic water splitting

As a result, considering the three main steps, good photocatalysts should possess these basic properties [14, 15]:

- (a) Optimum band gap energy (lower than 3 eV for visible-light absorption, but greater than the potential of the overall reactions of 1.23 eV)
- (b) Suitable band edge potentials for water splitting
- (c) Stability to chemical and environment

3.2 Bismuth vanadate photocatalyst

Bismuth vanadate, which formula is BiVO₄, is one of the intensively studied photocatalysts due to its attractive advantages: the number of studied on BiVO₄-based compounds increases exponentially over years as seen in Figure 2 [18].

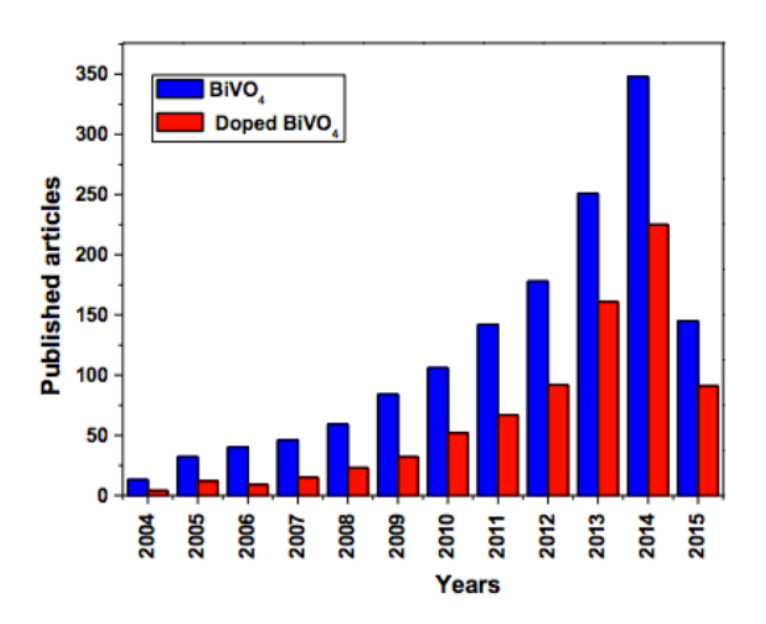


Figure 2. Number of publication on BiVO₄ based photocatalysts for 2004-2015 period [18]

One strategy to improve the BiVO₄ performance is band engineering. By modifying its orbitals, such as by substitutional doping, band edges can be altered. For BiVO₄, the conduction band edge of

BiVO₄ is dominated by the V 3d, O 2p, and Bi 6p [23]. Thus, to lift the conduction band edge, substitutional dopants should have a higher energy level atomic orbital than host lattices. For example, dopants on Bi site should have a higher energy level than the 6p orbital's. Also, dopants on V site should have a higher energy level than the 3d orbital's [24].

Previously, many studies have been focused on the effect of dopants on V site. Among the studied dopants, molybdenum is the most effective substitutional dopant on V site for a BiVO₄ photocatalytic system: the Mo-doped BiVO₄ photocatalyst exhibited the highest improved photocurrent [25]. As a result, Mo dopant is chosen to substitute on V site for this study. On the other hand, only few reports have been found on consequences of having impurities on Bi site. In addition, most studies on Bi site's doping show negative result or negligible improvement on photocatalytic activity. Only recently, a process to engineer the band edges of BiVO₄ by simultaneously doping on both Bi and V sites has been suggested by W.J. Jo et al [11]. It has been reported that In³⁺/Mo⁶⁺ dual doping triggers partial phase transformation from pure monoclinic BiVO₄ to a mixture of monoclinic and tetragonal BiVO₄, which essentially leads to an increase in compressive lattice strain, and consequently, band gap widening as well as an uplifting of CBE which enables H₂ evolution. In other words, by introducing the dopant atoms, the structure was under compressive strain resulting in a wider visible-light absorbing band gap and higher conduction band edge.

Even if BiVO₄ system with In³⁺/Mo⁶⁺ dual doping successfully generate hydrogen, studies on other doping systems are not fully explored. As a result, other options of doping systems are great of interest. In principles, hydrostatic strain has an important effect on the band structure of a semiconductor; it can shift the energetic position of

the band [23, 24]. Additionally, compressive and tensile strain results in different changes in band gap energy. Particularly in the case of silicon, a compressive hydrostatic strain causes an increase, whereas an expansive hydrostatic strain causes a decrease in band gaps [27]. Thus, as our strategy for orbital engineering, substitutional doping can induce strain and possibly leads to orbital modification, resulting in a change of the band edges. Moreover, different sizes, oxidation states and orbital energy levels can lead to a different change in the band structure. Also, for compatible substitution, all dopants should possess the same coordination number as Bi does, namely the coordination of eight.

Thus, in this study, the effect of strain affected by dopants on the hydrogen generation performance is investigated by altering dopants of the BiVO₄ system. The selection of appropriate dopants on Bi site is systematically studied by varying types of ionic dopant Ln in (Bi_{1-x}Ln_x)(V_{1-y}Me_y)O₄ where the choices of Ln ion are shown in Table 1, and Me = Mo or W. The sizes and the oxidation states of the doping ions decrease from the left to right columns, whereas the orbital energy levels increases from the first to second row [26, 27]. In order to compare the result of different dopants, the doping concentration is fixed to be 3 percent by mole. The necessity of having ion with p orbital to the uplifting of CBE is decided by comparing photocatalytic activity among all studied dopants to determine the suitable dopant for this compound.

Table 1. Data of Material of Selection (Ionic radii of the studied dopants (with a coordination number of VIII), Charge and Orbital energy)

Element	Y	In	Sn
Ionic radius* (Angstrom)	1.019	0.92	0.81
Charge	+3	+3	+4
Orbital energy	Low	High	High

^{*}Note: an ionic radii of Bi³⁺ (VIII) is 1.17 Angstrom.

Source: Database of Ionic Radii by the Atomistic Simulation Group in the Materials Department of Imperial College (http://abulafia.mt.ic.ac.uk/shannon/ptable.php)

4. Objectives

The ultimate goal of this study is to better understand how to improve the BiVO₄ performance by structure modification. This project is divided into three parts with specific objectives as follows

<u>Study 1</u>: The effect of doping on properties of non-stoichiometric BiVO₄ compounds

- (1) To investigate the effect of composition on BiVO₄
 photocatalytic activity: this is to obtain an insight of how
 dopants influence the local structure of non-stoichiometric
 BiVO₄ compounds and how that affect the photocatalytic
 performance
- <u>Study 2</u>: The effect of dual-doping on properties of BiVO₄ related compounds
 - (1) To investigate the effect of dual-doping on a phase formation of BiVO₄ photocatalysts with different stoichiometries, including the influence of doping type and doping concentration on changes of atomic structure
- and (2) To investigate the effect of dual-doping on BiVO₄ photocatalytic activity
- <u>Study</u> 3: The effect of heterostructure on BiVO₄ water splitting performance
 - (1) To investigate the effect of structure modification on BiVO₄ photocatalytic activity

5. Methodology

The study started with materials synthesis and preparation. Then, the samples were investigated for their physical properties, such as crystal structure and morphology, and their photocatalytic performance. The detail of each study according to the objectives are described as follows.

<u>Study 1</u>: The effect of doping on properties of non-stoichiometric BiVO₄ compounds

All compositions of the studied BiVO₄ compounds were synthesized via solid-state reaction route. Tungsten oxide was chosen as dopant in non-stoichiometric BiVO₄ compounds. The starting materials used for the synthesis were bismuth (III) oxide [Bi₂O₃, 99.99% purity], vanadium (V) oxide [V₂O₅, 99.99% purity] and tungsten (VI) oxide [WO₃, 99.998% purity] and all chemicals were of analytical reagent grade in a form of powder.

Table 3 shows the mole ratio of the starting materials used for synthesis of all metal-deficient BiVO₄ samples. The typical synthesis procedure was as follows: Bi₂O₃ and V₂O₅ powder were weighed according to a proper ratio of the non-stoichiometric compounds, namely Bi-deficiency and V-deficiency. The level of metal deficiency were varied: 3%, 6% and 12%, and denoted on the sample names. A certain mole of WO₃ was added into the mixture to compensate the deficit of the starting component. Then, the mixture was ground and ball-milled with an addition of ethanol and YSZ balls as grinding media for 24 hours at a speed of 60 rotations per minute. The mixture was then dried at 80°C for 6 hours and, after that, calcined at 650°C for 6 hours under the ambient atmosphere.

Table 3. The mole ratio of the starting materials used for syntheses

Sample	Type	Bi ₂ O ₃	V_2O_5	WO_3
Pure	Stoichiometry	1	1	-
3Bi	Bi-deficiency	0.97	1	0.06
6Bi	Bi-deficiency	0.94	1	0.12
12Bi	Bi-deficiency	0.88	1	0.24
3V	V-deficiency	1	0.97	0.06
6V	V-deficiency	1	0.94	0.12
12V	V-deficiency	1	0.88	0.24

The phase formation of the calcined powder was characterized using X-ray diffractometer. Prior to the measurement, the powder was mounted onto a sample holder. Powder X-ray diffraction (XRD, Phillip X'Pert) was operated at 45 kV and 40 mA with a Cu K α radiation (λ = 0.15418 nm) with no filter. The data was collected in a 2 θ range of 20-70°. The scan speed and the step size was 0.05 °/s and 0.02, respectively.

The morphologies of the as-synthesized powder were investigated using scanning electron microscopy (SEM, Philips XL30). The specific surface area was analyzed using a nitrogen adsorption-desorption measurement with a Micromeritics surface analyzer. To prepare the samples for surface area measurement, 250 mg of the sample was degassed at 220 ℃ for 4 hours. The specific surface area estimations were based on Brunauer-Emmet-Teller (BET) theory. The optical absorption spectra were obtained using a Shimadzu UV-vis spectrophotometer. The sample for UV-vis spectrophotoscopy was prepared by casting 1 g of the calcined powder mixed with PEG on a glass substrate and annealed at 400 ℃ for an hour. The absorption measurement was carried out in the wavelength range of 300 - 800 nm. The resultant optical absorption spectra were also used for band gap energy estimation.

The photocatalytic performance of the samples was determined by measuring the photocatalytic degradation of methylene blue (MB) aqueous solutions under UV-light irradiation. A 300W UV lamp (OSRAM) was used as a light source. Initially, 50 mL of MB aqueous solution (5mg/L) loaded with 0.2 g of the as-prepared BiVO₄ powder was stirred for 15 min in the dark to obtain the adsorption-desorption equilibrium before irradiation. After dark experiment, the suspension was exposed to the light and, during illumination, 3 mL of the solution was collected every fifteen minutes for 135 min. All the collected MB solutions were centrifuged at 75 rpm to remove the photocatalytic particles. The absorption spectra of the centrifuged MB solution was studied in the wavelength range of 300-700 nm using a UV-vis spectrometer (UV-1700, Shimadzu). The concentration ratio (C/C_0) was calculated to determine photodegradation activity of the dye at the maximum wavelength of $\lambda = 553$ nm (where C_0 is the initial concentration of MB and C is the concentration of MB at a given time).

<u>Study 2</u>: The effect of dual-doping on properties of BiVO₄ related compounds

All (Bi_{1-x}Ln_x)(V_{1-y}Mo_y)O₄ compounds were prepared using solidstate reaction. The main starting materials were Bi₂O₃, V₂O₅ and MoO₃. The dopant substances, namely SnO₂, In₂O₃, Y₂O₃, were added according to the chemical compositions. All starting materials were mixed stoichiometrically. The mixture was ball-milled for 24 hours and then heated in the furnace to 550°C for 5 hours to complete the reaction.

The obtained powder of the samples was yellow in color as shown in Figure 3. However, there was a variation in shade when the dopants and doping concentrations were altered. Typically, the color became darker when increasing doping concentration. This could be attributed to a change in optical band gap energy.



Figure 3. The obtained powder from the syntheses.

X-ray diffraction technique (XRD, Phillip X'Pert) was used to investigate a crystal structure of the synthesized powder. The X-ray diffractometer was operated at 45 kV and 40 mA with a Cu K α radiation ($\lambda = 0.15418$ nm) with no filter. The data was collected in a 2 θ range of 20-80°. To understand the valence state of the host lattice in the crystal structure, Synchrotron Radiation beamline at SLRI for XANES and EXAFS analyses were used. Plus, the morphologies and the surface area of the as-synthesized powder were investigated using scanning electron microscopy (SEM, Philips XL30) and a Micromeritics surface analyzer, respectively. In addition, the optical absorption spectra were obtained using a Shimadzu UV-vis spectrophotometer.

The synthesized materials were tested their photochemical properties in a closed system of a quartz reaction with 300W LED irradiation. The reaction vessel contains 0.1 g of sample dispersed in DI water using magnetic stirring with purged N₂ to remove dissolved gases. The investigation was conducted at room temperature under atmospheric pressure and gas sampling was conducted every 15 min using a syringe. The evolved gas was measured using a gas chromatography (Shimadzu).

The hydrogen production using the compounds with different compositions and morphology will be compared to determine the efficiency of each material system.

<u>Study 3</u>: The effect of heterostructure on BiVO₄ water splitting performance

The heterostructure of photoanode for this study is WO₃/BiVO₄. This structure was chosen because of its suitable band alignment. Specifically, the band alignment of WO₃/BiVO₄ could favor electron-hole transport and enhance a charge separation. The performance of the heterostructure photoanode was compared with the performance of a single BiVO₄ layer to evaluate the effect of electrode's structure on the water splitting performance.

A layer of WO₃ was obtained by spin-coating processes. First, a precursor solution was prepared by dissolving tungstic acid (H₂WO₄, Sigma-Aldrich, 6 mmol) into 1 M sulfuric acid (H₂SO₄, 98% purity, ACI labscan, 6 mL) and was stirred for 24 h until the solution was homogeneous. Then, 27% hydrogen peroxide (H₂O₂, Alfa Aesar) was added to obtain a clear solution. After that, the WO₃ precursor was spincoated onto the FTO glass substrates. The spin-coating process was repeated two times to increase film thicknesses. Finally, the films were calcined at 550 °C for 2 h with a heating rate of 10 °C/min. The WO₃/BiVO₄ photoanodes were prepared by spin coating BiVO₄ layers onto the predeposited WO₃ layer. For BiVO₄ deposition, a precursor prepared by dissolving ammonium metavanadate (NH₄VO₃, Daejung, 3 mmol) into 4 M nitric acid (HNO₃, 65% purity, Emsure, 10 mL). When the solution was stirred, bismuth nitrate pentahydrate (Bi(NO₃)₃.5H₂O₃, Daejung, 3 mmol) was added into the solution. After 3 h of stirring, the solution became yellowish. Then, citric acid (C₆H₈O₇, 6 mmol) was

added into the solution and stirred until the solution turned blue. The blue solution (6 mL) was then mixed with polyvinyl alcohol solution. This BiVO4 precursor solution was used for spin-coating processes. The mixture was dropped onto an FTO substrate with the prepared WO₃ layer. The spin was set at the first speed of 750 rpm for 10 s and the second speed of 4000 rpm for 25 s. After deposition, thermal treatment was conducted. The optimization of thermal treatment was also investigated. Four conditions were studied as denoted: W-BVO(NA, 400-0.5) was a sample with treatment condition of no preannealing treatment and annealing at 400 C for 30 min; W-BVO(A, 400-0.5) was a sample with treatment condition of preannealing treatment at 60 °C for 15 min and annealing at 400 °C for 30 min; W-BVO(NA, 400-5) was a sample with treatment condition of no preannealing treatment and annealing at 400 °C for 5 h; and W-BVO(NA, 400-5) was a sample with the treatment condition of preannealing treatment at 60 °C for 15 min and annealing at 400 °C for 5 h. Characterizations: The morphology of WO₃/BiVO₄ photoanodes was observed by SEM (FEI, Quanta450) equipped with an EDS used to analyze the film chemical composition. Phases of the samples were examined by XRD (Phillips X'pert) using Cu Kα radiation $(\lambda \frac{1}{4} 1.5418 \text{ Å})$. All patterns were recorded in the range of 15–80. The crystallite sizes of the samples were estimated using the Scherrer formula. The ultraviolet–visible spectrometer (UV-1700, Shimadzu) was used to measure the optical absorption of the prepared photoanodes (wavelength: 300–800 nm), and the optical bandgaps were calculated using the Tauc equation. PEC Measurement: PEC measurement was carried out by potentiostat/galvanostats (Autolab PGSTAT 302N) using a threeelectrode system. The WO₃/BiVO₄ photoanodes were used as a working electrode, Pt was used as a counter electrode, and Ag/AgCl and saturated KCl electrode was used as a reference electrode. In addition, an aqueous

solution containing $0.5~M~Na_2SO_4$ was used as an electrolyte. LSV was conducted to examine the PEC performance of the WO₃/BiVO₄ photoanodes. For the measurement, the applied voltage was varied from - 0.2~to~2.0~V~(vs~Ag/AgCl) at a scanning rate of 10~mV/s. Also, a 100~W LED was illuminated during the measurement.

6. Results and Discussion

6.1 Study 1: The effect of doping on properties of non-stoichiometric $BiVO_4$ compounds

All non-stoichiometric BiVO₄ compounds, namely Bi-deficient compositions and V-deficient compositions, doped with different amount of WO₃ were investigated for phase formation, morphology, band gap energy, and photocatalytic performance. The results are following.

Figure 4 (a) and (b) show the XRD spectra of the as-prepared compounds for Bi-deficient and Vi-deficient compositions, respectively, with various non-stoichiometry. The diffraction patterns were sharp indicating a high crystallinity of the samples. For the pure sample, the diffraction pattern was well indexed with a standard pattern of monoclinic scheelite BiVO₄ phase (JCPDS card no.14-0688). It should be noted that the pattern displays high intensity of diffraction peaks at 2θ of 34.513° and 35.239° of which are the characteristic peaks of monoclinic scheelite structure (m-BiVO₄) and can be used to distinguish monoclinic scheelite from tetragonal scheelite structure (t-BiVO₄).

Similar patterns were also observed in the Bi- and V-deficient compounds with low doping concentration (3Bi and 3V) meaning that monoclinic scheelite structure was obtained in both compositions. In addition, no extra peaks corresponding to impurity phases were detected. As the doping content was increased, the diffraction patterns altered. Specifically, for Bi-deficit samples, an impurity phase of WO₃ residue was found. Instead of incorporation of W in the structure, WO₃ remained in the Bi-deficit compounds and made the sample comprised of mixed phases of monoclinic scheelite and tungsten oxide. It should also be noted that the amount of WO₃ residue was increased as doping concentration increased. Meanwhile, in the case of the V-deficit compounds, increasing

the doping content led to a noticeable shift of the characteristic peaks. The spacing between the characteristic peaks became closer suggesting that the monoclinic phase (m-BiVO₄) possibly transformed to the tetragonal phase (t-BiVO₄). This is in good agreement with other literature.[30] Zhou et al. (2012) demonstrated that by modifying the BiVO₄ structure with dopants whose concentration exceeded 10 mol%, the monoclinic scheelite structure can transform to the tetragonal scheelite structure.[30] This could be explained that higher doping concentration induces strain in the monoclinic structure which can lead to a ferroelastic transformation.

According to the results, it reveals that doping in different non-stoichiometric environment, namely Bi-deficit and V-deficit causes different phase formation. The existence of WO₃ residue in Bi-deficient compounds, but not in V-deficient compounds suggests that dopants cannot easily replace on Bi site. In other words, dopants are more likely to substitute on V site than Bi site. This can be extrapolated by considering the environment of Bi and V sites in the structure. Bi atoms form BiO₈ dodecahedra, whereas V atoms form ViO₄ tetrahedra. The substitution of W on Bi site is less thermodynamically favourable. This also well agrees with the previously reported computational work by P.Pakeetood *et al.*[31]

As a result, in the Bi-deficit conditions, a residue of dopants was left in the system instead of being incorporated in the BiVO₄ structure. On the other hand, dopant can favourably substitute V site in VO₄ tetrahedra, which results in no WO₃ residue, and retaining the monoclinic structure. However, the substitution of W on V site can cause an internal strain because W ion (0.059 nm) has a slightly larger radius than V ion (0.054 nm). Hence, when the substitutional doping of W increases, the internal strain is increased and, when the doping concentration is much

higher, such internal strain can drive a phase transformation of the monoclinic scheelite structure to the tetragonal scheelite structure.

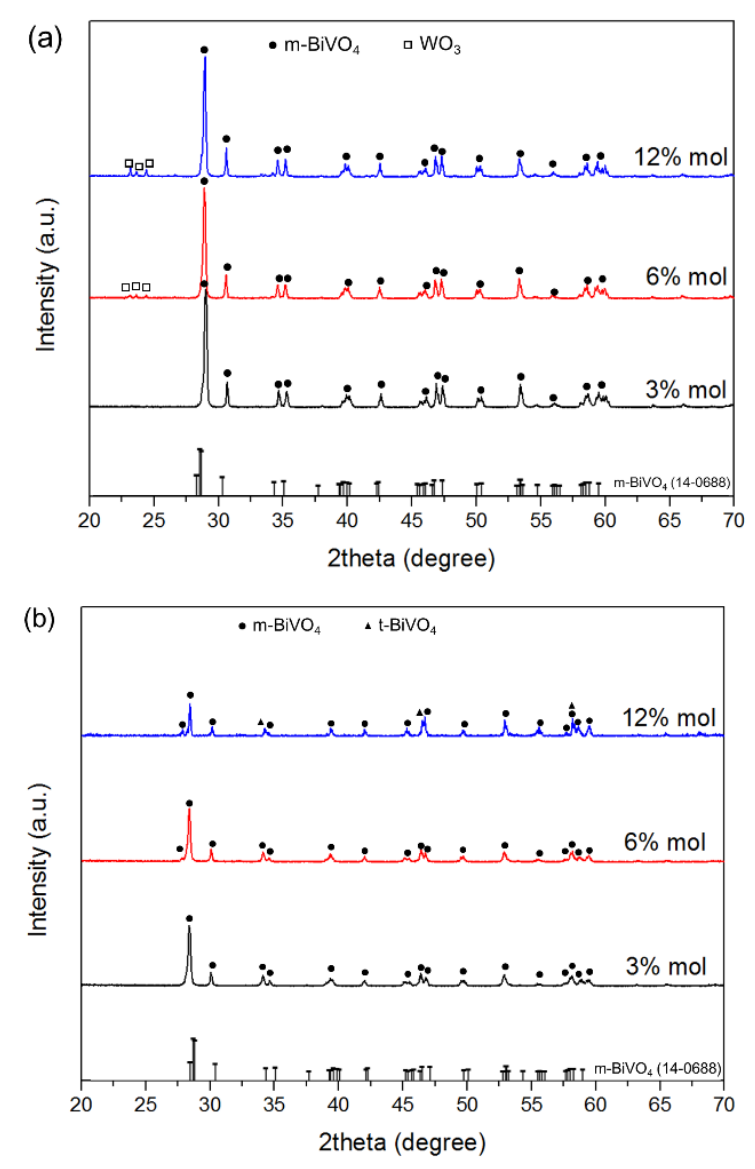


Figure 4. X-ray diffraction patterns of (a) Bi-deficient compositions and (b) V-deficient compositions

The morphologies of Bi- and V-deficit compounds were studied using scanning electron microscopy (SEM). Figure 5 (a), (b) and (c) demonstrate SEM images of the Bi-deficit compounds, while Figure 5 (d), (e) and (f) demonstrate SEM images of the V-deficit compounds.

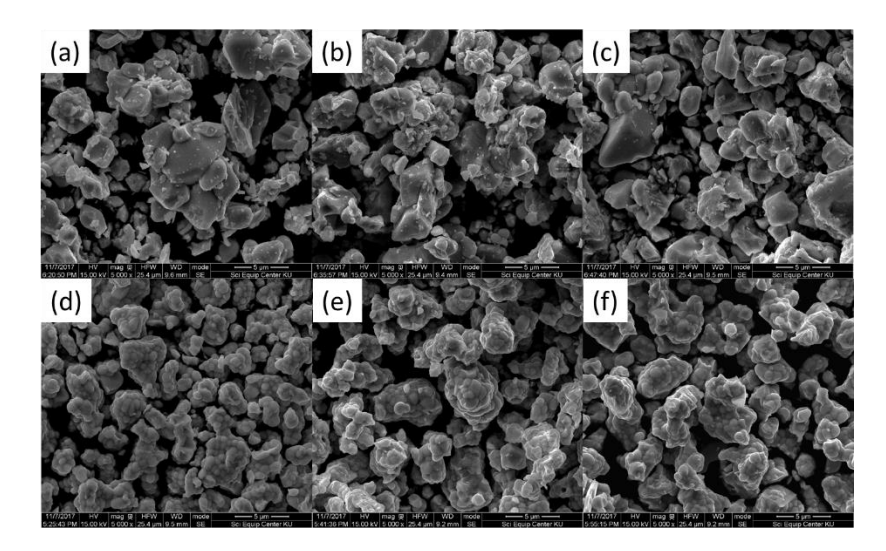


Figure 5. SEM micrographs of Bi-deficient compounds doped with (a) 3 mol%W (b) 6 mol%W and (c) 12 mol%W, and V-deficient compounds doped with (d) 3 mol%W (e) 6 mol%W and (f) 12 mol%W.

The size and shape of the as-synthesized powders with various compositions were different. For pure BiVO₄, the average size of powders was approximately 5.43 um and its surface were quite smooth. As the dopants were added, the particles became finer in size for both Bideficient and V-deficient compounds. Moreover, it was found that in the V-deficient compositions, the surfaces were rough which was resulted from agglomeration of small particles becoming large particles. The dissimilarities in size and particle formation between pure and non-stoichiometric BiVO₄ could be owing to dopants. Dopants can stimulate a nucleation which resulted in finer crystals and rough surfaces.

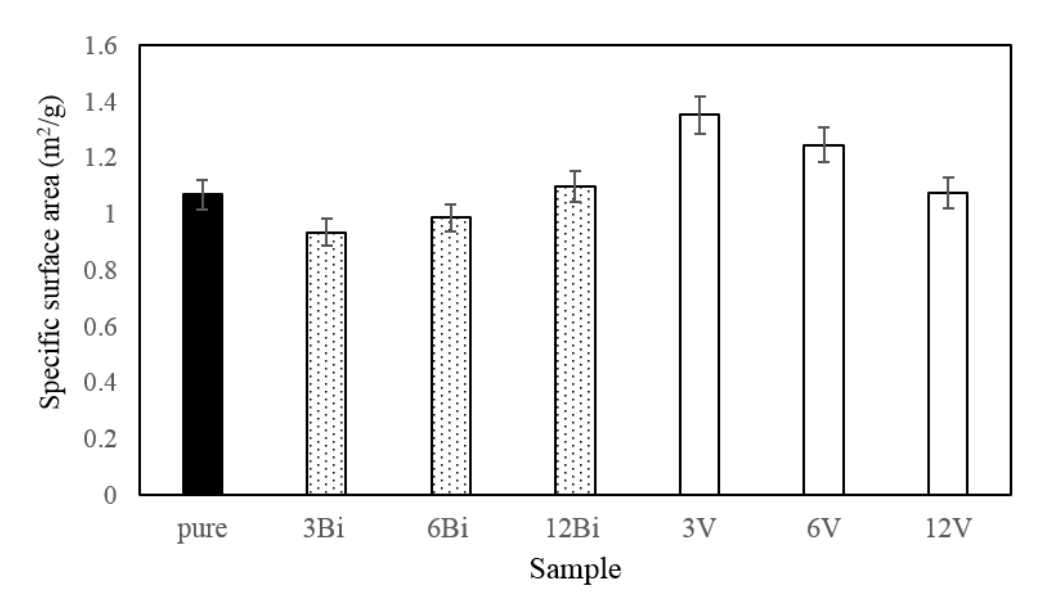


Figure 6. Specific surface area of the as-synthesized samples

In addition to morphology, specific surface areas of the assynthesize compounds were analysed by a Micromeritics surface analyzer based on Brunauer-Emmet-Teller (BET) estimation and are compared in Figure 6. The specific surface areas of the Bi deficient compounds were slightly lower, while the specific surface areas of the V deficient compounds than pure substance. The higher surface areas of the V deficient compounds can be attributed to the surface roughness of the agglomerated particles. As the doping concentration increased, the agglomeration became larger, so the specific surface area was decreased.

The optical absorption of all samples was measured using UV-vis spectrophotometer. The absorption spectra are displayed in Figure 7. All samples show high absorption in a range of UV and visible region. Such absorption spectra were also used to estimate band gap energy. The band gap was calculated according to the Tauc equation according to Kubelka-Munk theory are shown as an inlet in Figure 7. The band gap energies of non-stoichiometric compounds were larger than pure BiVO₄. However, when increasing the doping contents, the band gap became smaller. The

alteration of band gap energy could be induced by changes in defect population.

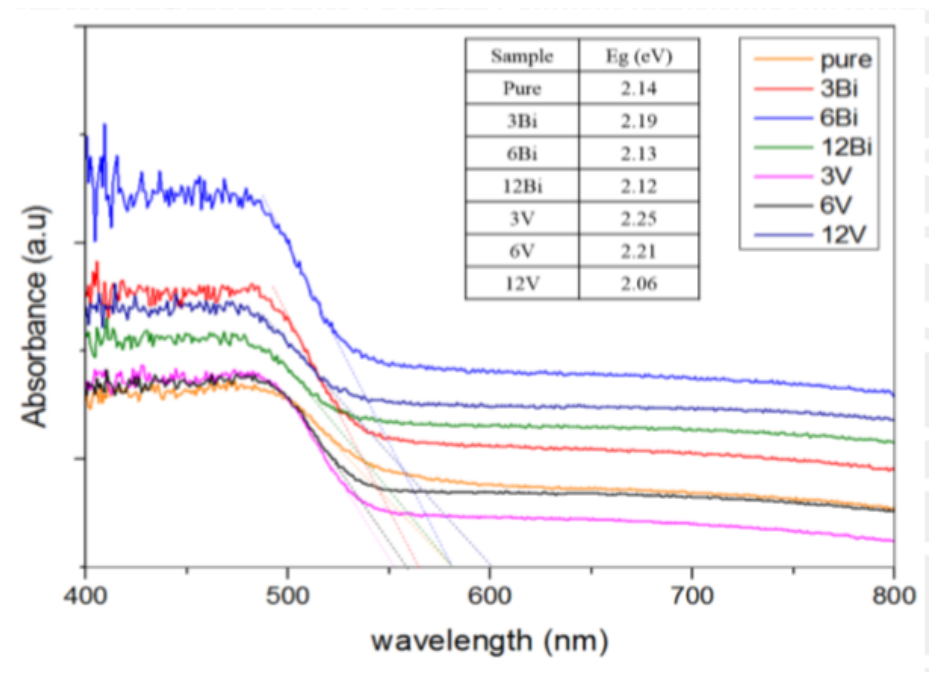


Figure 7. Tauc plot for band gap estimation

Photocatalytic performance of non-stoichiometric compounds
Photocatalytic activity of the prepared powder was examined by
photodegradation of MB under UV-light irradiation. After light
irradiation, photogenerated electrons and holes react with chemicals in
solution and create radicals which actively discolor methylene blue.
Figure 8 illustrates the percentage of photodegradation of MB using
various compositions of BiVO₄ photocatalysts after the UV irradiation for
120 min. The results showed that Bi-deficient compounds exhibited better
photocatalytic properties even if they possessed less specific surface areas
and comparable band gaps to the others. This result could be influenced
by the existence of the WO₃/BiVO₄ heterostructure. Due to the
heterojunction band alignment, the heterostructure can promote a charge
separation efficiency resulting in the enhanced photocatalytic activity. For
V-deficient compounds, the photocatalytic degradation dropped when the
doping concentration was 12 mol%. This performance decline could be

attributed to the presence of tetragonal scheelite phase which generally performs worse than monoclinic scheelite phase. In addition, defects created by dopants could act as recombination centers which further lower the photocatalytic activity of MB degradation.

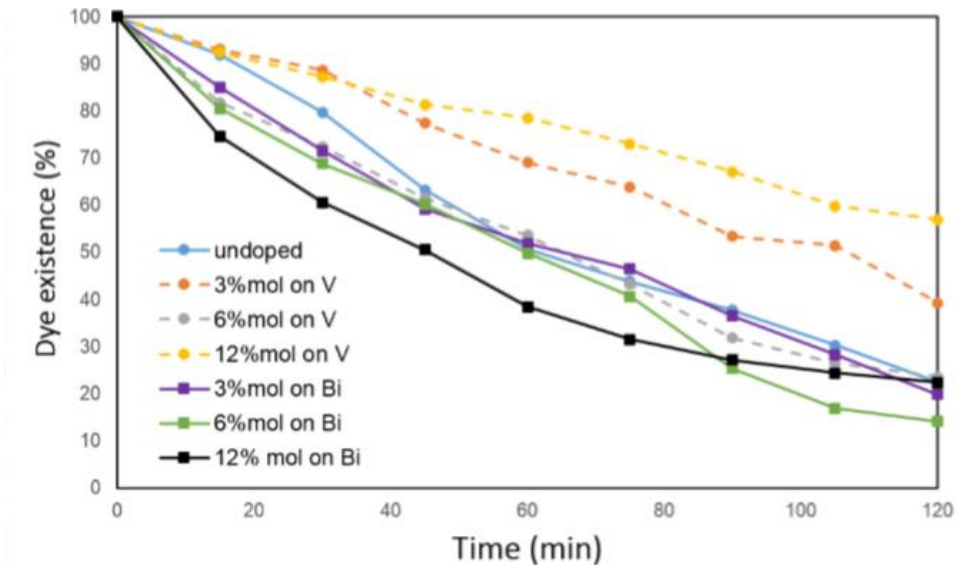


Figure 8. Photodegradation of methylene blue after UV irradiation for 120 min over pure and non-stoichiometric BiVO₄ compounds

A deeper explanation can be postulated based on the recent report of the computational study by J. T-Thienprasert (2019). Intrinsic defects were systematically investigated in BiVO₄. It has revealed that vacancies were dominant defects in BiVO₄. Typically, BiVO₄ comprises donor oxygen vacancy defects (V_0) and acceptor bismuth vacancy defects (V_{Bi}) and both defects are compensated. However, different synthesis conditions could lead to different nature of defects. Similar defects (V_0 and V_{Bi}) were observed in Bi-deficient compounds, while an addition of Bi interstitials was also found in V-deficient compounds. This could absolutely clarify the comparable photocatalytic performance in Bi-deficient composition and the lower photocatalytic activity in V-deficient composition compared to BiVO₄ stoichiometric compound which can be attributed to the formation of Bi interstitials.

6.2 Study 2: The effect of dual-doping on properties of BiVO₄ related compounds

The compounds of $(Bi_{1-X}Ln_X)(V_{0.97}Mo_{0.03})O_4$ where Ln = In, Sn, Y and x = 1, 3 and 5 at% were examined their structure and phase formation using an X-ray diffractometer. The results were shown in Figure 9-11.

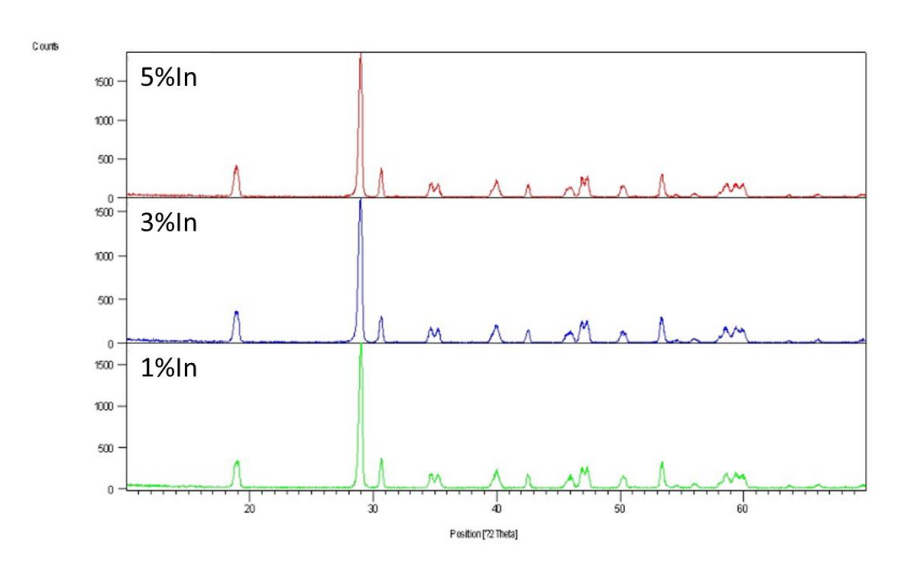


Figure 9. XRD pattern of the $(Bi_{1-X}In_X)(V_{0.97}Mo_{0.03})O_4$ compounds with different doping concentration of In

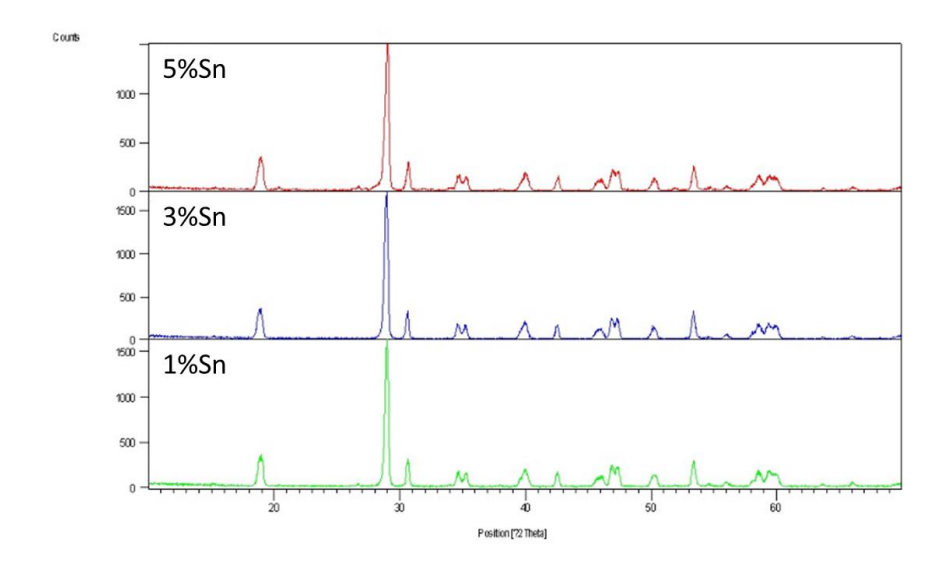


Figure 10. XRD pattern of the $(Bi_{1-X}Sn_X)(V_{0.97}Mo_{0.03})O_4$ compounds with different doping concentration of Sn

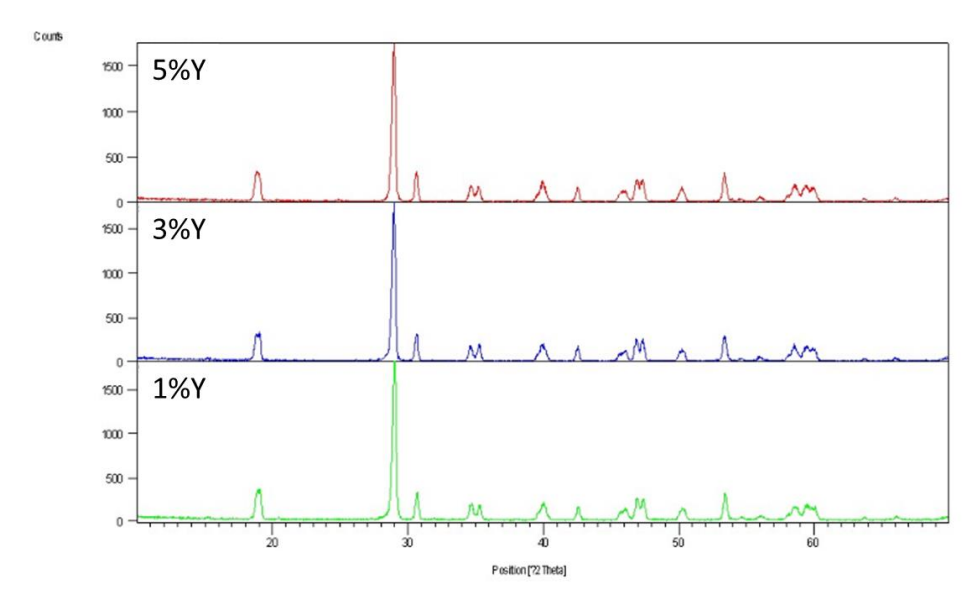


Figure 11. XRD pattern of the $(Bi_{1-X}Y_X)(V_{0.97}Mo_{0.03})O_4$ compounds with different doping concentration of Y

The XRD results revealed that all samples possessed monoclinic scheelite structure because the XRD patterns were in good agreement with a standard JCPDS no. 01-083-1699. However, it is noted that when doping concentration was increased for some compositions, the peaks of 34.89° and 35.1° became closer. This indicates that the obtained powder was mixed with tetragonal scheelite phase. In addition, there was a trace of impurities for 5% Sn doped compounds. This is because a high doping concentration and a small radius of Sn²⁺ can cause high internal strain in the structure leading in difficulty of substitutional defects.

The morphology of the samples was examined by a scanning electron microscope. The undoped $BiVO_4$ sample as shown in Figure 12 significantly had a larger average particle size than the other compositions (Figure 13 – 15). When dopants were added, the nucleation was easier to occur. As a result, smaller particle sizes were obtained. However, some dopant atoms could lead to an agglomeration causing a large particle formation with rough surfaces.

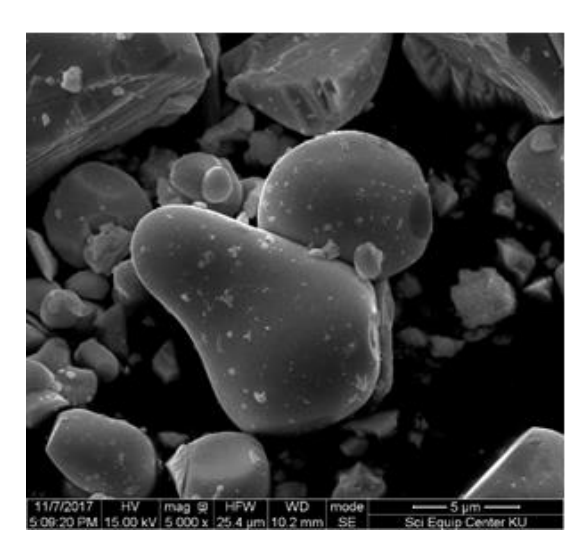


Figure 12. Morphology of undoped BiVO₄. Scale bar is 5 um.

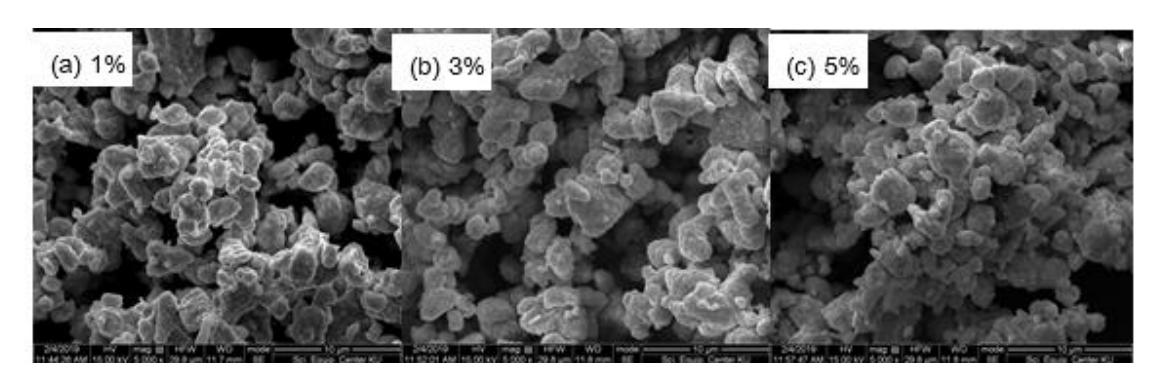


Figure 13. Morphology of In-doped BiVO₄. Scale bar is 10 um.

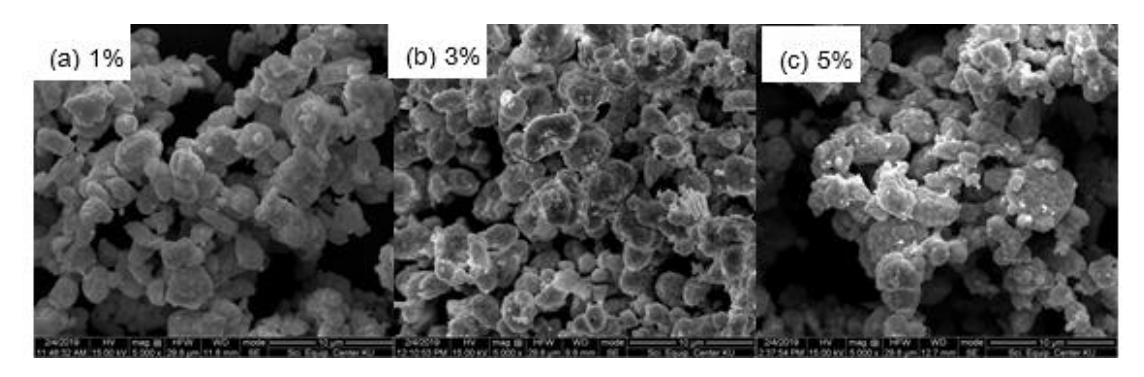


Figure 14. Morphology of Sn-doped BiVO₄. Scale bar is 10 um.

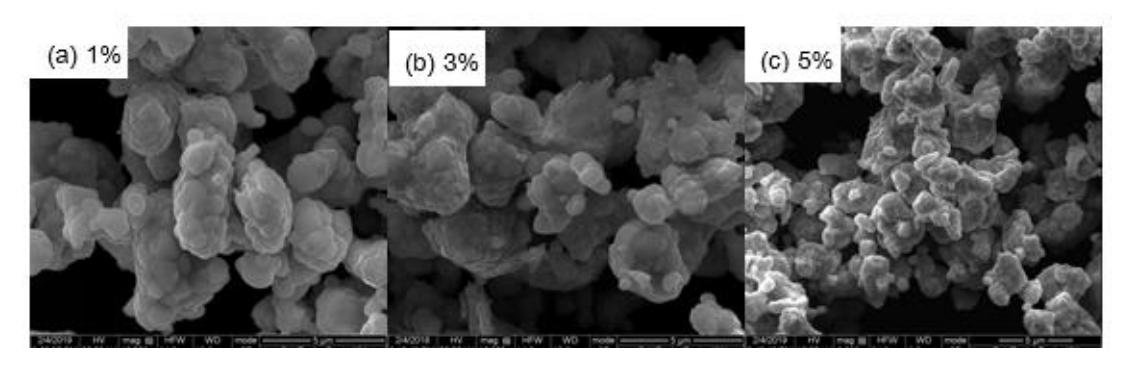
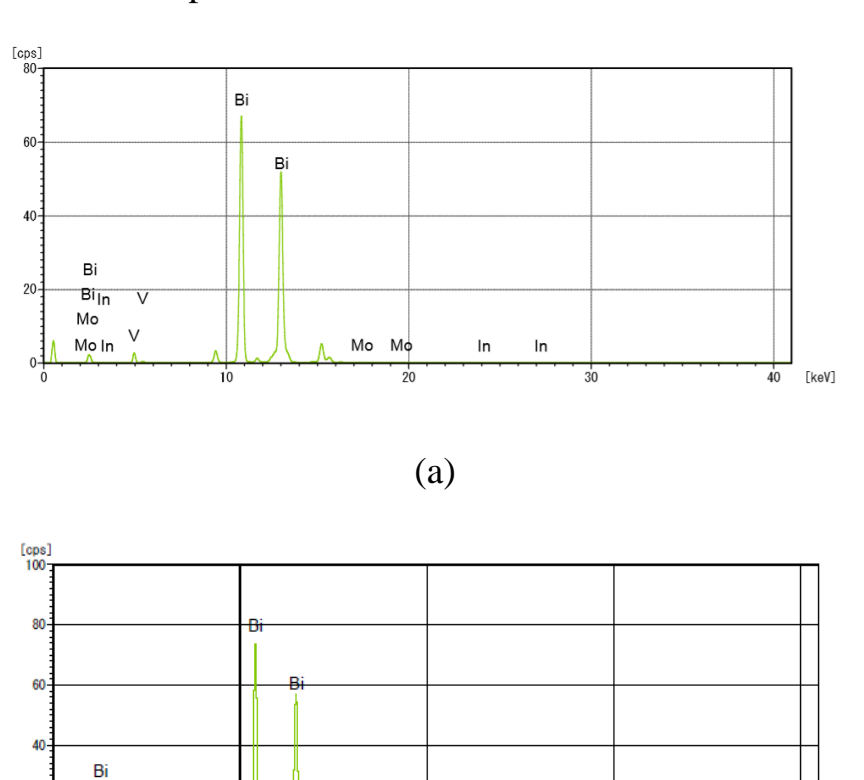


Figure 15. Morphology of Y-doped BiVO₄. Scale bar is 10 um.

The compositions of the samples were also investigated using an X-ray fluorescence technique. The results were shown in Figure 16. It can detect the small amount of dopants and the results confirm the element contained in the samples.



(b)

Sn

Sn

[keV]

Mo Mo Sn V

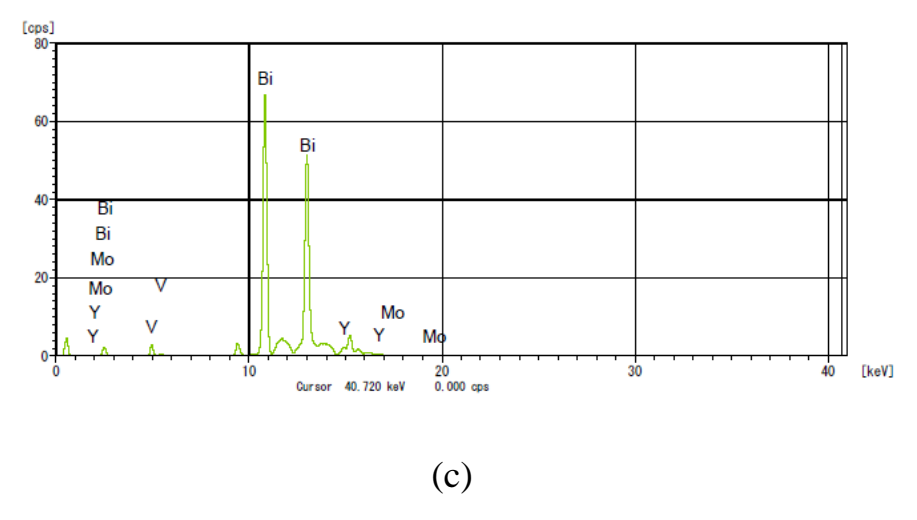
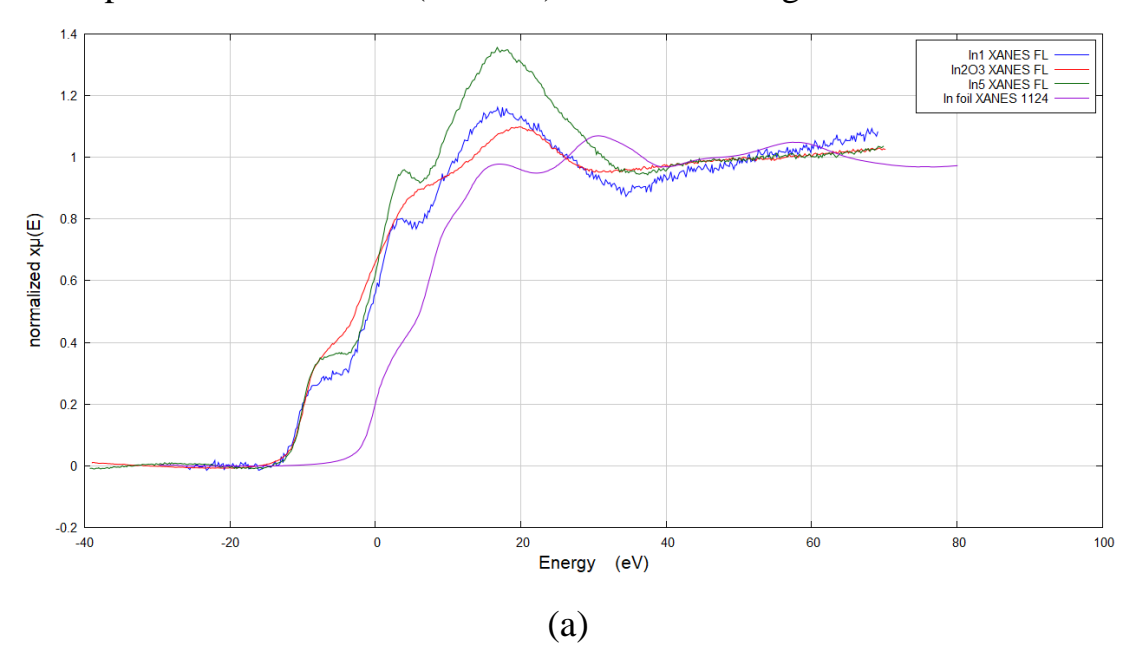


Figure 16. Elemental analysis of doped $BiVO_4$ powder (a) In, (b) Sn and (c) Y

The doped samples were further investigated using X-ray Absorption Near Edge Spectroscopy (XANES) and Extended X-Ray Absorption Fine Structure (EXAFS) as shown in Figure 17.



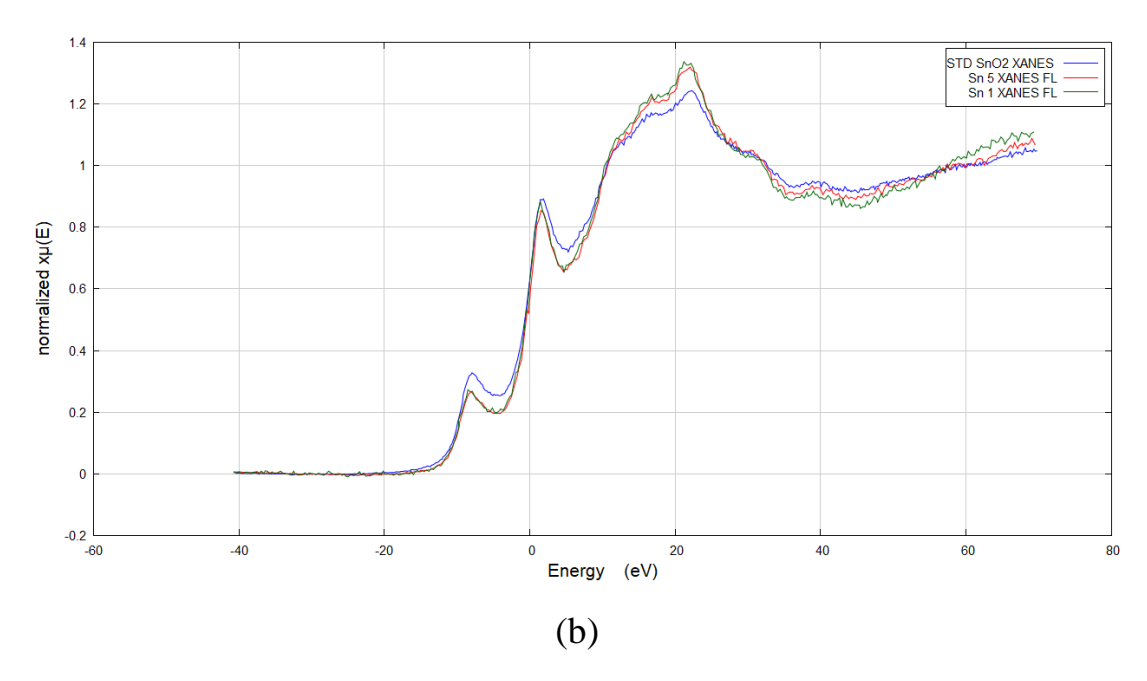


Figure 17. XAS spectra for XANES and EXAFS analyses

To obtain the information about the local structure of BiVO₄, FEFF fitting was analyzed to fit the EXAFS spectra at both the Bi and V edges. Information on coordination number (N), amplitude reduction factor (S_0^2) , Debye-Waller factor (σ^2) and interatomic distances (R) were presented in Table 4.

Table 4. Structural parameters obtained from XANES and EXAFS fitting analyses

Sample	Scattering path	N	S_0^2	σ^2	ΔΕ	R	R-factor
	V-O(1)	4	0.75	0.004	4.431	1.755	
	V-O(2)	2	0.75	0.018	4.431	2.857	
Sn1	V-O(3)	2	0.75	0.012	4.431	3.370	0.004
SIII	V-Bi(1)	4	0.75	0.006	4.431	3.686	0.004
	V-Bi(2)	2	0.75	0.005	4.431	3.999	
	V-Sn	1	0.75	0.000	4.431	3.951	
Sn5	V-O(1)	4	0.72	0.006	-1.279	1.735	
	V-O(2)	2	0.72	0.008	-1.279	2.765	
	V-O(3)	2	0.72	0.004	-1.279	2.991	0.008
	V-Bi(1)	4	0.72	0.014	-1.279	3.881	
	V-Bi(2)	2	0.72	0.002	-1.279	4.091	

	V-Sn	1	0.72	0.002	-1.279	3.719	
	V-O(1)	3	0.77	0.000	3.154	1.744	
	V-O(2)	2	0.77	0.002	3.154	3.008	
In1	V-O(3)	2	0.77	0.002	3.154	3.315	0.015
1111	V-Bi(1)	4	0.77	0.014	3.154	3.697	0.013
	V-Bi(2)	2	0.77	0.020	3.154	4.025	
	V-In	1	0.77	0.007	3.154	3.354	
	V-O(1)	4	0.78	0.004	2.171	1.742	
	V-O(2)	2	0.78	0.002	2.171	2.744	
In5	V-O(3)	2	0.78	0.003	2.171	2.980	0.006
1113	V-Bi(1)	4	0.78	0.014	2.171	3.741	0.000
	V-Bi(2)	2	0.78	0.005	2.171	4.003	
	V-In	1	0.78	0.006	2.171	3.344	

From the analyses, it shows a good fitting with the data. In addition, it demonstrates that increasing doping concentration decreases bonding in the local structure. It also shows that the local environment of BiVO₄ with any dopant elements is not symmetric. This distortion could cause an internal polarization improving a charge separation.

The specific surface area of the samples was analyzed by using a Brunauer, Emmett and Teller (BET) technique. The results are shown in Table 5 and reveal that the specific surface area is compositional dependent. Doping with different elements causes differences in surface area. Moreover, altering doping contents also causes a slight change in its surface area.

Table 5. Specific surface area of the samples using BET technique

Dopant	Doping content (%mol)	BET surface area (m ² /g)
In	0.01	1.1410
	0.03	1.1253
	0.05	1.1513
Sn	0.01	0.8502
	0.03	1.1792
	0.05	1.4081
Y	0.01	1.4760
	0.03	1.3236
	0.05	1.6443

The photocatalytic water splitting performance of all samples was determined using a photoreactor under 100W LED illumination. The evolved gas was sampled every 30 min and measure the amount of gases using gas chromatography. The result for 5% Sn-doped sample was shown in Figure 18.

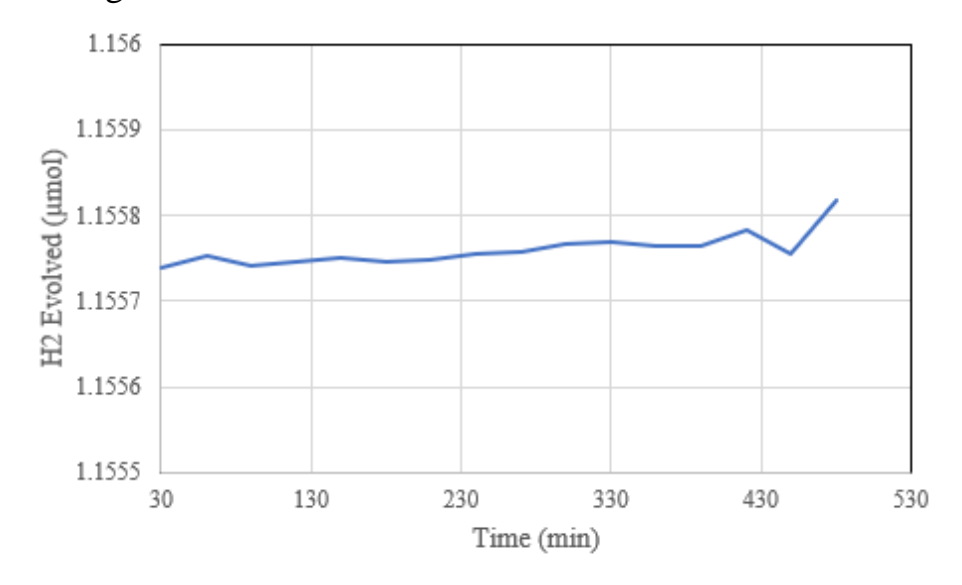


Figure 18. H₂ evolution detected from 5%Sn-doped sample

The result reveals that the evolved H_2 was difficult to detect with this method. As a result, the procedure for determining photocatalytic performance was adjusted. Specifically, the pellet sample of each compound was prepared, and its PEC performance was investigated using a potentiostat. The result was shown in Figure 19.

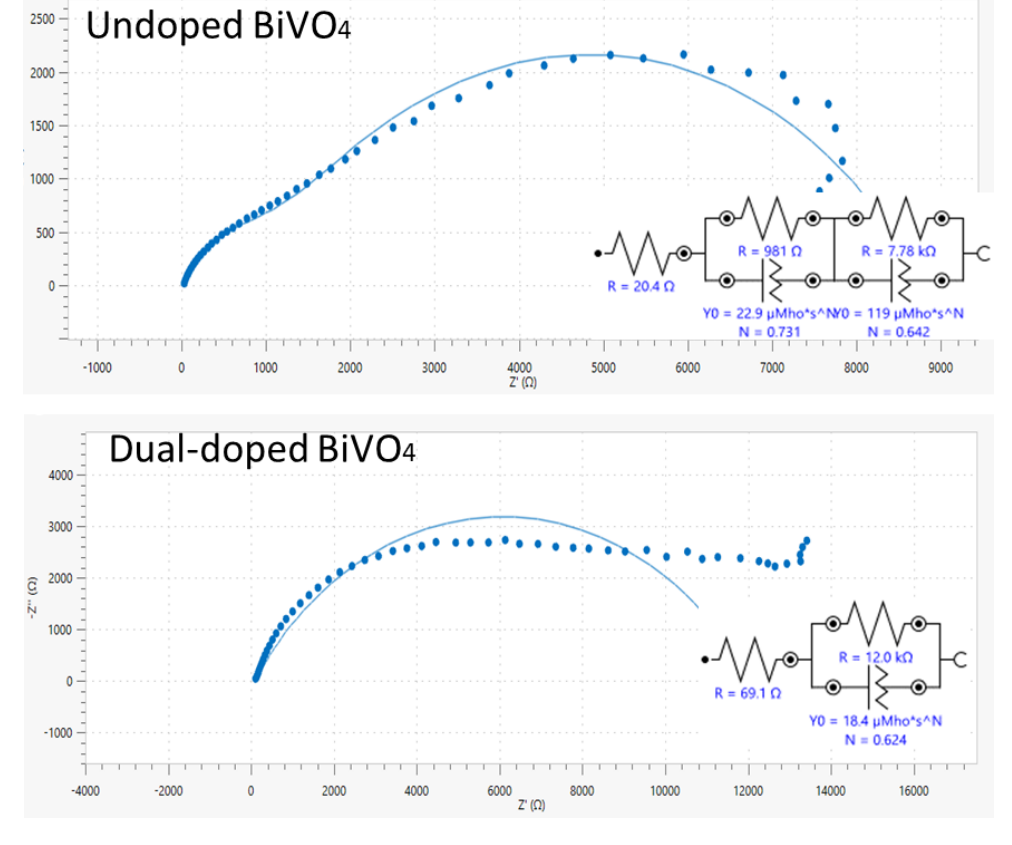


Figure 19. Comparison of photoelectrical performance for water splitting of undoped and dual-doped samples

The PEC performance compared between undoped and dual-doped samples revealed that dual-doped samples possessed significantly lower resistance, implying that dual-doped BiVO₄ has a better kinetics for water splitting. This also means a better performance for water splitting for dual-doped samples.

In addition, the photocatalytic performance of all samples was investigated by photodegradation efficiency of MB. The sample was added into aqueous MB solution and then the sample was irradiated under a UV light. The photodegradation of MB by the sample was measured every 15 minutes using a UV-vis spectrophotometer and the result was shown in Figure 20.

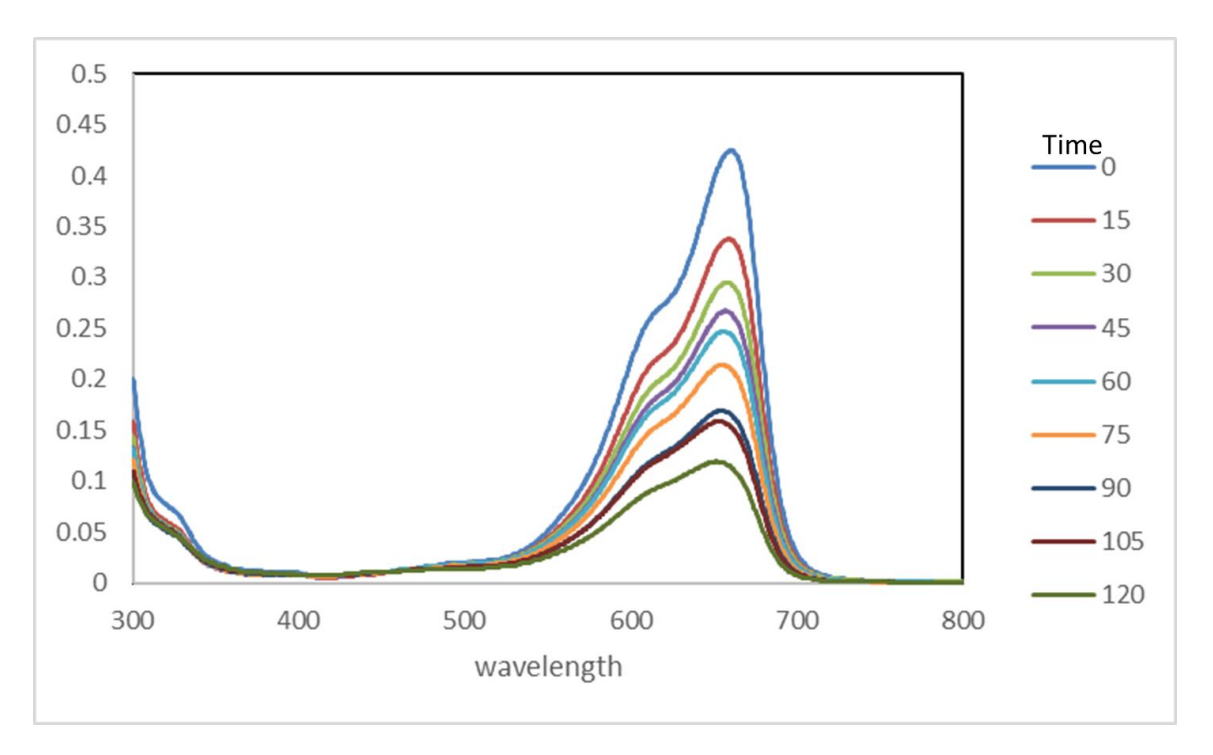


Figure 20. Dye degradation at different time

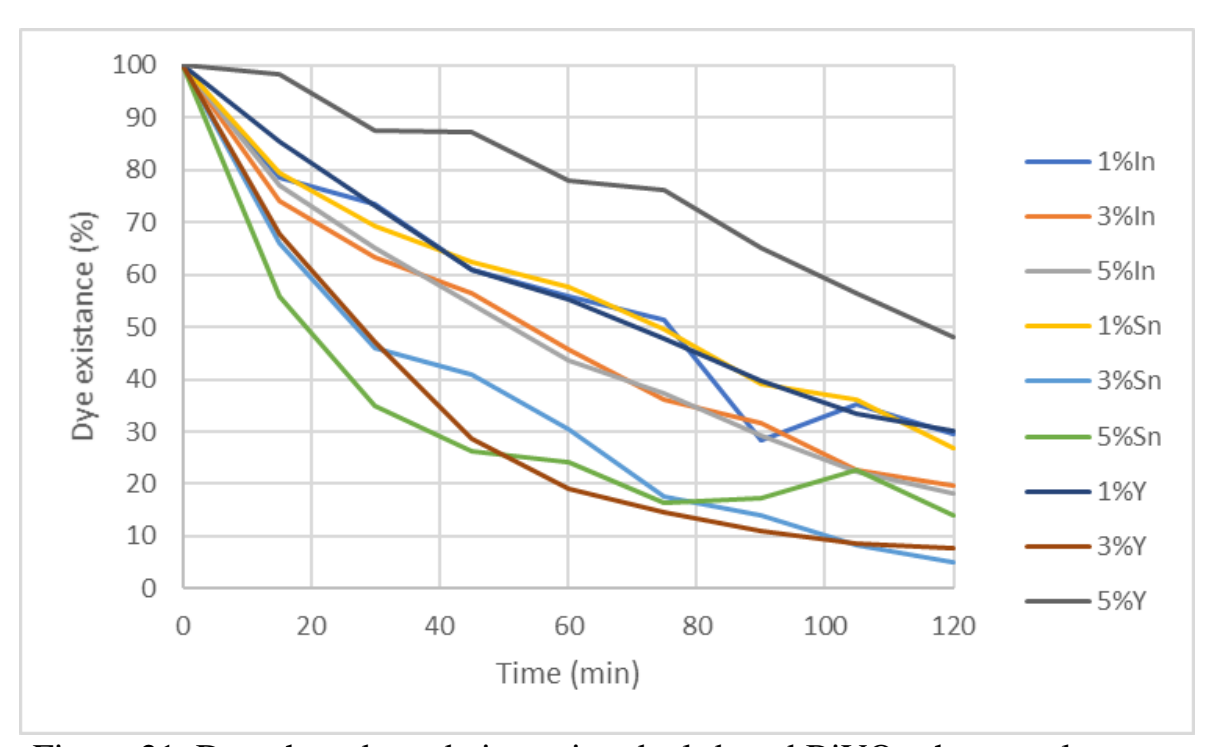


Figure 21. Dye photodegradation using dual-doped BiVO₄ photocatalyst

Dye degradation results (Figure 21) show that typically increasing doping concentration can increase photocatalytic activity. However, (Y,Mo)-doped BiVO₄ did not show the same expectation. This might be

explained by morphology of the sample. Y-dual doped powder was agglomerated. As a result, it could lead to a recombination of charge carriers resulting in lower performance. Among all, Sn-doped samples seem to have a good performance.

6.3 Study 3: The effect of heterostructure on BiVO₄ water splitting performance

Phase formation of the eterojunction photoanodes prepared by spin-coating method onto FTO substrate with different thermal treatment was characterized using an X-ray diffractometer. Figure 22 demonstrates the XRD results of all prepared photoanodes. The diffraction patterns exhibited peaks at 18.9°, 28.9° and 34.4° which can be indexed as a phase of monoclinic scheelite BiVO₄ (JCPDF no.14-0688).

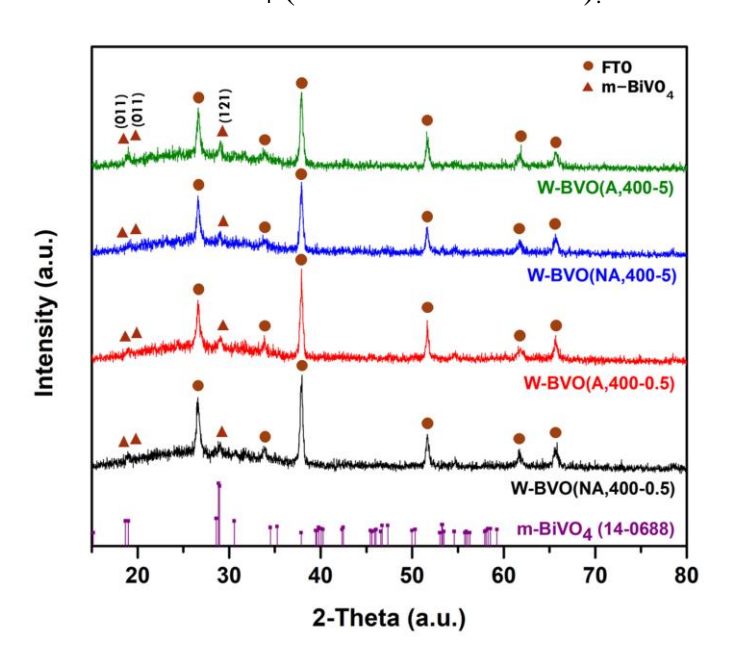


Figure 22. XRD pattern of WO₃/BiVO₄ heterojunction thin film photoanode

Additionally, the other peaks belonged to the FTO substrate denoted with circle symbols. It should be noted that the diffraction pattern of the WO₃ layers could not be observed. This is possibly due to the small

thicknesses of the WO₃ layers which were beyond the detection limit of the X-ray diffractometer. As a result, energy dispersive spectroscopy (EDS) was used to determine the formation of the tungsten oxide layer. In addition to the phase formation analyses, the full width half maximum (FWHM) and the crystalline size were calculated based on the diffraction peak at 28.9°. The results showed that the pre-annealing strongly influenced the morphology and crystallinity of the film. The samples underwent the pre-annealing step had a larger crystalline size. In other words, the pre-annealing step led to a significant increase in crystalline size.

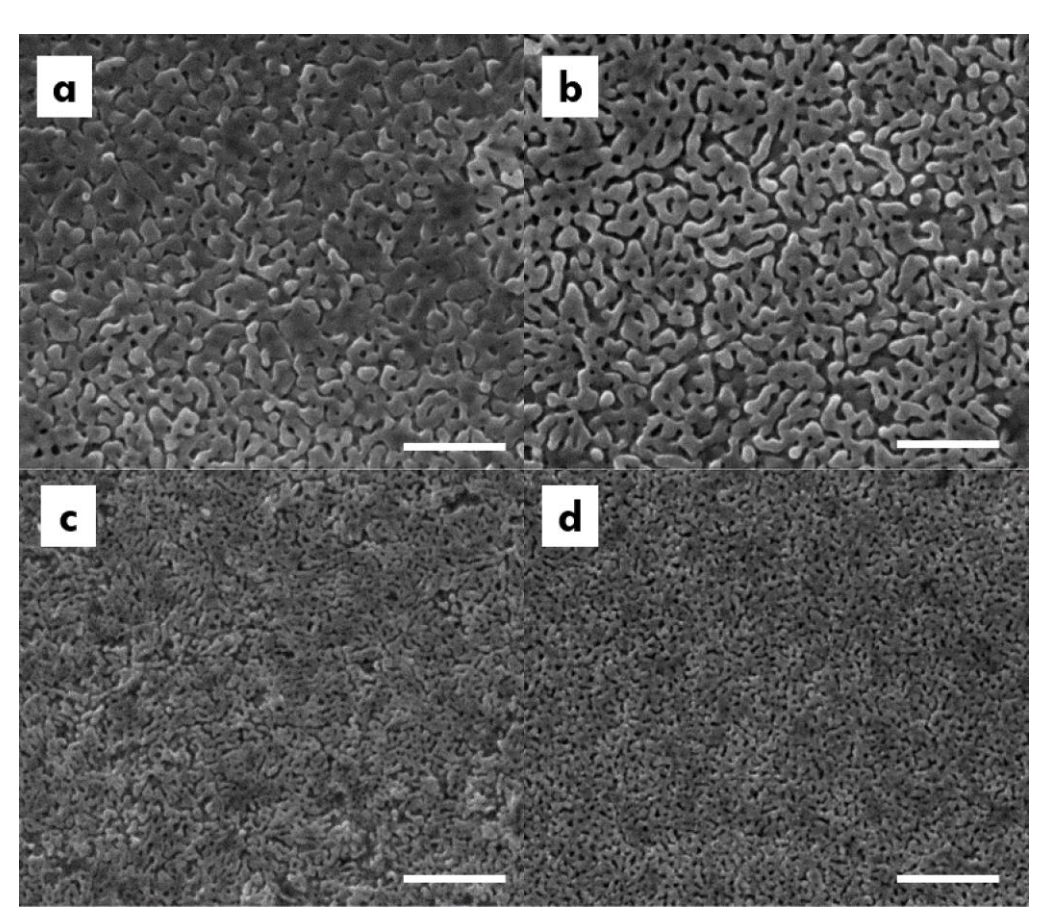


Figure 23. SEM image of $WO_3/BiVO_4$ heterojunction thin film photoanodes (a) W-BVO(400,5), (b) W-BVO(60,15-400,5), (c) W-BVO(400,30) and (d) W-BVO(60,15-400,30)

The morphologies of WO₃/BiVO₄ heterojunction thin film photoanodes were investigated by scanning electron microscopy. The SEM micrographs shown in Figure 23 demonstrated that all films possessed a network structure. However, under different thermal treatment conditions, the width of the interconnected structure was altered. Increasing annealing time can widen the width of the structure. As a result, the films with 5-hour annealing revealed a larger width of the network structure. Moreover, compared with no pre-annealed samples, the pre-annealed films were less dense and possessed a better uniformity with evenly distributed pores and spacing. This higher porosity and uniformity may be attributed to a gradual evaporation of precursor solution during a pre-annealing process.

The optical absorption behaviours of the WO₃/BiVO₄ heterojunction thin film photoanodes were investigated using UV–vis spectrophotometer. The results are presented in Figure 24. All samples exhibited a strong absorption within a range of 430-480 nm with an absorption edge at approximately 480 nm as shown in Figure 24(a). However, the samples with pre-annealing showed an improved absorption ability even though the films were thinner. This could be explained by the high uniformity and crystallinity of the films. In addition, this finding also implies that controlling a quality of films, namely uniformity and crystallinity, could significantly improve optical properties.

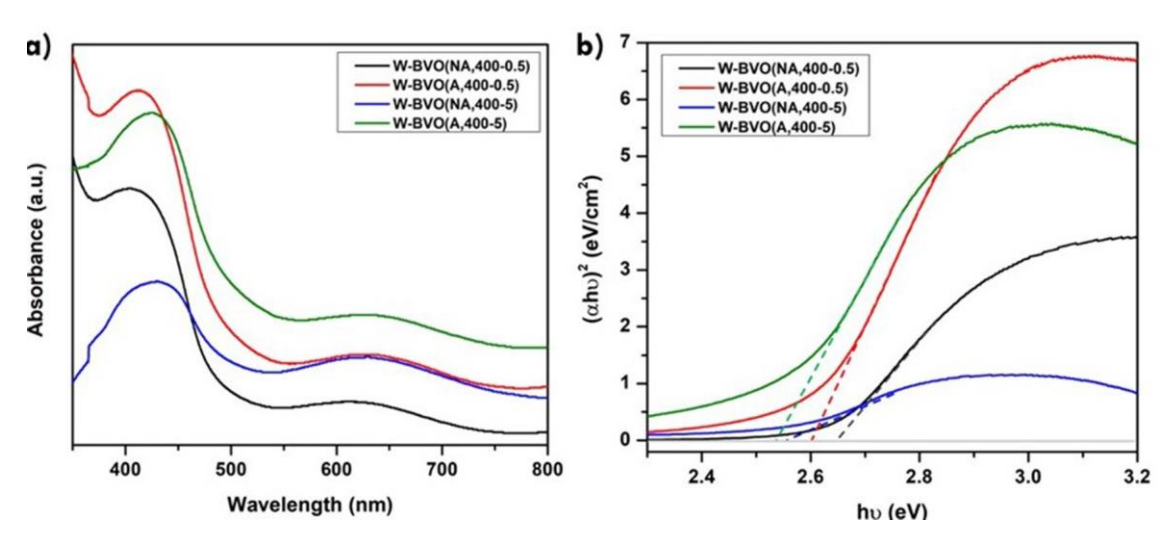


Figure 24. (a) UV-VIS absorption spectra and (b)Tauc plot of WO₃/BiVO₄ heterojunction thin film photoanodes

The Tauc plot of the WO₃/BiVO₄ heterojunction photoanodes revealed that the band gap values of the samples were slightly different. The samples with pre-annealing process demonstrated slightly decreased band gaps. In addition, among all samples, W-BVO(60,15-400,5) exhibited the smallest band gap. Even though the band gaps were slightly different, the values were still at around 2.5 eV which is comparable with previous literatures.

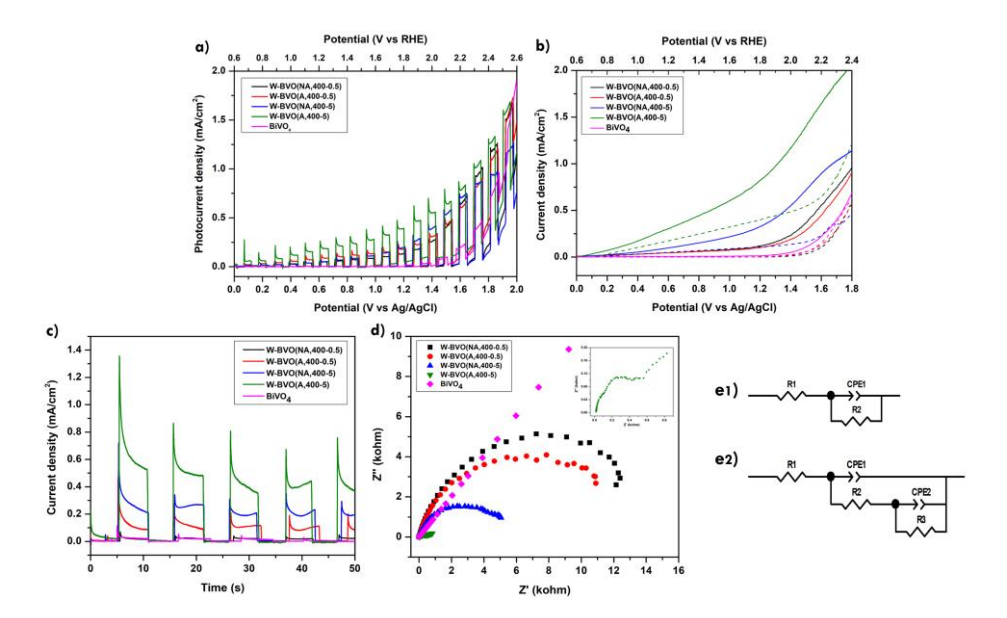


Figure 25. (a) The LSV curve (b) the LSV curve compared with dark and light, (c) the chopped It curve at a constant applied potential of 1.23 V (vs Ag/AgCl), (d) the Nyquist plots of WO3/BiVO4 heterojunction thin film photoanodes

The photoelectrochemical performance of the photoanodes was investigated using a potentiostat equipped with a standard three-electrode system and an illumination of 100W LED light source and is depicted in Figure 25. The linear sweep voltammetry (LSV) curves in Figure 25(a) show that the photocurrent density was enhanced with a pre-annealing treatment. The photocurrent density at 1.23 V vs Ag/AgCl in 0.5 M Na₂SO₄ solution was 2.4, 0.27, 0.18, and 0.13 mA/cm² for W-BVO(60,15-400,5), W-BVO(400,5), W-BVO(60,15-400,30) and W-BVO(400,30), respectively. As a result, the samples with a pre-annealing step and longer annealing time, namely W-BVO(60,15-400,5), exhibited the best photoelectrochemical performance. This observation also corresponded to the onset potential showing that the sample of W-BVO(60,15-400,5) obtained the lowest value. This implies that the W-

BVO(60,15-400,5) sample requires the lowest potential to activate a reaction.

The high PEC performance of the W-BVO(60,15-400,5) sample could be associated with its film characteristics. Specifically, large width, high uniformity and high porosity of interconnect-structured films are advantageous for photochemistry. These features provide larger surface area for reaction sites resulting in an increased photoactivity. It should be also noted that, among all films, this film possessed the highest absorption ability and the thinnest thickness which could result in the largest population of photogenerated carriers as well as a higher possibility for charge carriers to reach the electrolyte/electrode interface suggesting favorable attributes for higher photocurrent density.

Figure 25(b) compares the photocurrent density under dark condition and light irradiation. It reveals that all samples were photo-responsive. Moreover, when the light was illuminated, electrons and holes were generated, and photocurrent density was increased. In addition, time-dependent photocurrent response under a condition of chopped illumination was illustrated in Figure 25(c). The result showed a noticeable spike of photocurrent density when the light was on. Then, a rapid decay in photocurrent density was observed before reaching a steady state. This could be related to a charge recombination before the surface reaction. Further, when the light was switched off, the photocurrent was back to zero.

The PEC performance of the WO₃/BiVO₄ heterostructure photoanodes was also compared with the one of a single BiVO₄ layered photoanode. The results demonstrated that the heterostructure significantly improved the PEC performance. This could be speculated that heterostructure enhances a charge separation. In general for photoanodes, after electrons and holes are generated, electron will travel

inwards a semiconductor or towards an electron collector, while holes will travel towards an electrolyte. WO₃/BiVO₄ heterojunction consists a band structure which could assist an electron-hole separation. The conduction band of the WO₃ layer is more positive than that of the BiVO₄ layer. Similarly, the valence band of the WO₃ layer is also more positive than that of the BiVO₄ layer. The band alignment is favorable for electrons to migrate towards the WO₃ layer, and for holes to travel outwards the BiVO₄ electrolyte interface.

In addition, water oxidation kinetics at the photoanode /electrolyte interface were evaluated by FRA impedance mode with a three electrodes system immersed in Na₂SO₄ electrolyte. The results revealed the R_{ct} values of 110.4 ohm, 4.2×10^3 ohm, 11.7×10^3 ohm and 13.2×10^3 ohm for W-BVO(60,15-400,5), W-BVO(400,5), W-BVO(60,15-400,30) and W-BVO(400,30) photoanodes, respectively. Among all, the W-BVO (60,15-400,5) exhibited the smallest R_{ct} value which was in good agreement with its PEC performance. Due to its efficient charge transfer, the W-BVO(60,15-400,5) sample showed the better photoelectrochemical efficiency.

7. Conclusions

The project shows strategies to improve photocatalytic properties of BiVO₄ compounds aimed of seawater splitting by dual-doping. The study provides an insight of the effect of doping on properties nonstoichiometric BiVO₄ compounds which is important to modify the structure. The result demonstrated that adding dopants in various nonstoichiometry can cause different phase formation. Also, the dopants strongly affected morphology. Specifically, dopants which successfully substitute in the structure could lead to more nucleation resulting in higher surface area. Moreover, in this study, the phase formation was a strong contributor to photocatalytic performance. Bi-deficient BiVO₄ compounds exhibits a high yield of photodegradation due to the occurrence of dopant residue which possibly promotes a charge separation. In the meantime, for V-deficient compounds, dopants generated defects in the structure which could generate more recombination centers resulting in recombination of photogenerated electrons and holes before they can involve in further step of photocatalytic processes. The lower activity can be strongly attributed to defect and phase formation. The results suggest that controlling composition (by either non-stoichiometric or doping synthesis) can strategically manipulate photocatalytic properties.

Dual-doped BiVO₄ compounds were synthesized via a solid state reaction. These compounds have a formulation of (Bi₁₋ $_{X}Ln_{X}$)(V_{0.97}Mo_{0.03})O₄ where Ln = In, Sn, Y and x = 1, 3 and 5 at%. X-ray diffraction results reveal that all compounds possessed a monoclinic sheelite structure. However, some impurities were found for 5% Sn doped sample. This is possibly because a large size mismatch between Sn and Bi atom which can cause a high internal strain and high energy structure. As

a result, it is more difficult for Sn to substitute in the host lattice. Moreover, the local structure analyses show that all local environment was asymmetrical. This could cause a local polarization which facilitates a charge separation. In addition, it was found that dual-doped with Sn and Mo exhibited a good photocatalytic performance compared to the others.

In addition to local structure modification, the cell structure modification was considered. The heterostructure of WO₃/BiVO₄ was fabricated and compared the photoelectrochemical performance with a single layer of BiVO₄. It was found that sample preparation was key to get a good performance. Specifically, the samples with pre-annealing and annealing steps showed higher photocurrent. This is because such preparation steps improve the morphology, namely the surface area and uniformity of the heterostructure. As a result, the better performance of the heterostructure are contributed to three factors, namely an enhanced charge population mainly due to the film quality, an improved charge separation due to the heterostructure, and an efficient charge transfer due to the smaller interfacial resistance.

For future investigation, the film heterostructure would be a potential candidate because it shows a promising result from the preliminary study. In addition, the film structure will be easy to use in many applications and easy to fabricate as well. Moreover, simluation study would be an area of interest to predict the performance and support the experimental studies.

References:

[1] "Thailand energy report 2015." [Online]. Available: http://www.eppo.go.th/index.php/en/energy-information-services/report-2015. [Accessed: 03-Sep-2016].

- [2] Y. Fan, D. Li, M. Deng, Y. Luo, and Q. Meng, "An overview on water splitting photocatalysts," *Front. Chem. China*, vol. 4, no. 4, pp. 343–351, Nov. 2009.
- [3] S. M. Ji, H. Jun, J. S. Jang, H. C. Son, P. H. Borse, and J. S. Lee, "Photocatalytic hydrogen production from natural seawater," *J. Photochem. Photobiol. Chem.*, vol. 189, no. 1, pp. 141–144, Jun. 2007.
- [4] W. Luo *et al.*, "Solar hydrogen generation from seawater with a modified BiVO₄ photoanode," *Energy Environ. Sci.*, vol. 4, no. 10, pp. 4046–4051, Sep. 2011.
- [5] "A light-assisted, polymeric water oxidation catalyst that selectively oxidizes seawater with a low onset potential Chemical Science (RSC Publishing)." [Online]. Available: http://pubs.rsc.org/en/Content/ArticleLanding/2013/SC/c3sc50812a #!divAbstract. [Accessed: 03-Sep-2016].
- [6] Y. Li *et al.*, "Efficient and Stable Photoelectrochemical Seawater Splitting with TiO₂@g-C₃N₄ Nanorod Arrays Decorated by Co-Pi," *J. Phys. Chem. C*, vol. 119, no. 35, pp. 20283–20292, Sep. 2015.
- [7] J. A. Seabold, K. Zhu, and N. R. Neale, "Efficient solar photoelectrolysis by nanoporous Mo:BiVO₄ through controlled electron transport," *Phys. Chem. Chem. Phys.*, vol. 16, no. 3, pp. 1121–1131, Dec. 2013.
- [8] K. Ding, B. Chen, Z. Fang, Y. Zhang, and Z. Chen, "Why the photocatalytic activity of Mo-doped BiVO₄ is enhanced: a comprehensive density functional study," *Phys. Chem. Chem. Phys.*, vol. 16, no. 26, pp. 13465–13476, Jun. 2014.
- [9] S. P. Berglund, A. J. E. Rettie, S. Hoang, and C. B. Mullins, "Incorporation of Mo and W into nanostructured BiVO₄ films for

- efficient photoelectrochemical water oxidation," *Phys. Chem. Chem. Phys.*, vol. 14, no. 19, pp. 7065–7075, Apr. 2012.
- [10] A. Kudo, K. Ueda, H. Kato, and I. Mikami, "Photocatalytic O2 evolution under visible light irradiation on BiVO₄ in aqueous AgNO₃ solution," *Catal. Lett.*, vol. 53, no. 3–4, pp. 229–230.
- [11] W. J. Jo *et al.*, "Phase transition-induced band edge engineering of BiVO₄ to split pure water under visible light," *Proc. Natl. Acad. Sci. U. S. A.*, vol. 112, no. 45, pp. 13774–13778, Nov. 2015.
- [12] K. Maeda, "Photocatalytic water splitting using semiconductor particles: History and recent developments," *J. Photochem. Photobiol. C Photochem. Rev.*, vol. 12, no. 4, pp. 237–268, Dec. 2011.
- [13] A. Kudo and Y. Miseki, "Heterogeneous photocatalyst materials for water splitting," *Chem. Soc. Rev.*, vol. 38, no. 1, pp. 253–278, 2009.
- [14] R. Abe, "Recent progress on photocatalytic and photoelectrochemical water splitting under visible light irradiation," *J. Photochem. Photobiol. C Photochem. Rev.*, vol. 11, no. 4, pp. 179–209, Dec. 2010.
- [15] K. Maeda and K. Domen, "New Non-Oxide Photocatalysts Designed for Overall Water Splitting under Visible Light," *J. Phys. Chem. C*, vol. 111, no. 22, pp. 7851–7861, Jun. 2007.
- [16] X. Guan, F. A. Chowdhury, N. Pant, L. Guo, L. Vayssieres, and Z. Mi, "Efficient Unassisted Overall Photocatalytic Seawater Splitting on GaN-Based Nanowire Arrays," *J. Phys. Chem. C*, Feb. 2018.
- [17] "Selectivity between Oxygen and Chlorine Evolution in the Chlor-Alkali and Chlorate Processes Chemical Reviews (ACS Publications)." [Online]. Available:

- https://pubs.acs.org/doi/10.1021/acs.chemrev.5b00389. [Accessed: 09-Mar-2018].
- [18] V. I. Merupo, "Synthesis and characterization of metal doped BiVO₄ nanostructured materials for photocatalytic applications," phdthesis, Université du Maine, 2016.
- [19] R. Li *et al.*, "Spatial separation of photogenerated electrons and holes among {010} and {110} crystal facets of BiVO₄," *Nat. Commun.*, vol. 4, p. 1432, 2013.
- [20] R. Munprom, P. A. Salvador, and G. S. Rohrer, "Polar Domains at the Surface of Centrosymmetric BiVO₄," *Chem. Mater.*, vol. 26, no. 9, pp. 2774–2776, 2014.
- [21] R. Munprom, P. A. Salvador, and G. S. Rohrer, "Ferroelastic domains improve photochemical reactivity: a comparative study of monoclinic and tetragonal (Bi_{1-0.5x}Na_{0.5x})(V_{1-x}Mo_x)O₄ ceramics," *J. Mater. Chem. A*, vol. 4, no. 8, pp. 2951–2959, Feb. 2016.
- [22] K. Ding, B. Chen, Y. Li, Y. Zhang, and Z. Chen, "Comparative density functional theory study on the electronic and optical properties of BiMO₄ (M = V, Nb, Ta)," *J. Mater. Chem. A*, vol. 2, no. 22, pp. 8294–8303, May 2014.
- [23] J. K. Cooper *et al.*, "Electronic Structure of Monoclinic BiVO₄," *Chem. Mater.*, vol. 26, no. 18, pp. 5365–5373, Sep. 2014.
- [24] A. Walsh, Y. Yan, M. N. Huda, M. M. Al-Jassim, and S.-H. Wei, "Band Edge Electronic Structure of BiVO₄: Elucidating the Role of the Bi s and V d Orbitals," *Chem. Mater.*, vol. 21, no. 3, pp. 547–551, Feb. 2009.
- [25] K. P. S. Parmar, H. J. Kang, A. Bist, P. Dua, J. S. Jang, and J. S. Lee, "Photocatalytic and photoelectrochemical water oxidation over metal-doped monoclinic BiVO₄ photoanodes," *ChemSusChem*, vol. 5, no. 10, pp. 1926–1934, Oct. 2012.

- [26] C.-C. Ren, W.-X. Ji, C.-W. Zhang, P. Li, and P.-J. Wang, "The effects of biaxial strain and electric field on the electronic properties in stanene," *Mater. Res. Express*, vol. 3, no. 10, p. 105008, 2016.
- [27] X. Peng, A. Alizadeh, S. K. Kumar, and S. K. Nayak, "Ab-initio Study of Size and Strain Effects on the Electronic Properties of Si Nanowires," *ArXiv10101556 Cond-Mat Physicsphysics*, Oct. 2010.
- [28] J. B. Mann, T. L. Meek, and L. C. Allen, "Configuration Energies of the Main Group Elements," *J. Am. Chem. Soc.*, vol. 122, no. 12, pp. 2780–2783, Mar. 2000.
- [29] R. N. Keller, "Energy level diagrams and extranuclear building of the elements," *J. Chem. Educ.*, vol. 39, no. 6, p. 289, Jun. 1962.
- [30] D. Zhou, H. Bin, J. Guo, L. Pang, Z. Qi, T. Shao, Q. Wang, Z. Yue, Z. Yao, "Phase Evolution and Microwave Dielectric Properties of (Bi $_{1-x}$ Fe $_x$)VO $_4$ ($x \le 0.40$) Ceramics," *J. Am. Cer. Soc.*, vol. 97, p. 2915, Sep. 2014.
- [31] P.Pakeetood, P. Reunchan, A. Boonchun, S. Limpijumnong, R. Munprom, R.Ahuja, J. T-Thienprasert, "Hybrid-Functional Study of Native Defects and W/Mo-Doped in Monoclinic-Bismuth Vanadate," *J. Phy. Chem. C*, vol. 123, p.14508, May. 2019.

8.Output (Acknowledge the Thailand Research Fund)

8.1 International Journal Publication

- S. Phiankoh, P. Prajongtat, M. Chareonpanich, **R. Munprom***, "The Improved Photoelectrochemical Performance of WO₃/BiVO₄ Heterojunction Thin-Film Photoanodes via Thermal Treatment," *J. En. Tech.*, vol.8, p. 2000147, Mar. 2020. DOI: 10.1002/ente.202000147 (IF: 3.175 (2017))

8.2 Research Utilization and Application

The knowledge from the project was used for academic purpose. Specifically, this new knowledge was taught in a class of Materials Engineering Department, Kasetsart University.

8.3 Others (international conference, book chapter, patent)

The results from the project were presented in international conferences as follows:

- "The Improved Photoelectrochemical Performance of WO₃/BiVO₄ Heterojunction Thin-Film Photoanodes via Thermal Treatment," The 2nd MRS-Thailand Conference 2019. July 10 12, 2019.
- "Doping effect on phase formation and photocatalytic properties of non-stoichiometric BiVO₄ compounds" The 8th Asia-Pacific Congress on Catalysis. Aug. 4-7, 2019.

Appendix International Journal Publication

The Improved Photoelectrochemical Performance of WO₃/BiVO₄ Heterojunction Thin-Film Photoanodes via Thermal Treatment

Soriya Phiankoh, Pongthep Prajongtat, Metta Chareonpanich, and Ratiporn Munprom*

Improvement in the photoelectrochemical (PEC) performance of WO₃/BiVO₄ heterojunction photoanodes is achieved by thermal treatment. The heterostructure systems consist of WO3 and BiVO4 layers spin coated onto fluorinedoped tin oxide (FTO)-coated glass substrates. The morphology and optical properties are modified by varying annealing conditions and calcining time. The crystal structure, morphology, and optical properties are studied using X-ray diffraction (XRD), scanning electron microscopy (SEM), and UV-vis spectroscopy, respectively. The results show that the WO₃/BiVO₄ photoanodes obtain an interconnected structure which helps promote the PEC activity by increasing the active area for reaction and shortening the distance for carrier diffusion. Also, the preannealing treatment can improve film qualities, namely crystallinity, uniformity, and optical absorbance, leading to an enhancement of the PEC performance. The optimal thermal treatment is preannealing at 60 °C for 15 min, followed by calcining at 400 °C for 5 h. The photoanode with such an optimal treatment exhibits the highest photocurrent density under light-emitting diode (LED) illumination, and the efficiency is increased by 3-4 times compared with the others. Herein, a simple method is offered to improve the PEC performance of a heterojunction photoelectrode.

1. Introduction

An energy insufficiency is one of the global issues that may be encountered in the future. With the rapid development of

S. Phiankoh, Dr. R. Munprom Department of Materials Engineering Faculty of Engineering Kasetsart University

50 Ngamwongwan Rd., Chatuchak, Bangkok 10900, Thailand E-mail: fengrtpm@ku.ac.th Dr. P. Prajongtat

Department of Materials Science Faculty of Science Kasetsart University 50 Ngamwongwan Rd., Chatuchak, Bangkok 10900, Thailand Prof. M. Chareonpanich Department of Chemical Engineering Faculty of Engineering Kasetsart University 50 Ngamwongwan Rd., Chatuchak, Bangkok 10900, Thailand

The ORCID identification number(s) for the author(s) of this article can be found under https://doi.org/10.1002/ente.202000147.

DOI: 10.1002/ente.202000147

industrialization and an increase in population driving to expansion in energy needs, this problem becomes more severe and it may come sooner than expected. [1,2] Therefore, it is necessary to find alternative energy sources to substitute the current use of limited fossil fuels.[3] The requirements of alternative energy that should be considered are cleanliness, affordability, harvesting/conversion efficiency, and sustainability.[4]

Hydrogen is considered as one of our hopes for alternative fuels. Hydrogen is an abundant element and can be found in many organic compounds, such as water and petrochemicals. Moreover, hydrogen fuel contains the highest energy density per mass. One kilogram of hydrogen fuel can produce $\approx 120 \,\mathrm{MJ}$ energy, which is three times higher than energy produced from the equivalent amount of gasoline.^[5] More importantly, its combustion is zero emission which makes hydrogen gas attractive as an efficient and clean fuel.[6]

Photoelectrochemical (PEC) water splitting is a technology to produce hydrogen fuel. The system utilizes semiconductor photoelectrodes and solar energy to convert water to hydrogen fuel. This energy conversion becomes one of the widely studied research areas because it can sustainably supply clean chemical energy. [7-9] The conversion process involves three crucial steps that can limit efficiency: 1) electron-hole generation, 2) electron-hole separation, and 3) electron-hole utilization. Many researchers are intensively attempting to improve the overall photoelectrochemical (PEC) performance by simply improving efficiencies of the three steps in the process. Research works have profoundly been devoted to developing novel photoelectrodes with excellent light-absorbing ability, aimed to enhance electron-hole generation. For example, many visible-light responsive oxides, such as Cu_2O ($E_g=2.17\,\text{eV}$), $^{[10]}$ Fe_2O_3 ($E_g=2.2\,\text{eV}$), $^{[11]}$ and BiVO_4 ($E_g=2.4\,\text{eV}$), $^{[12]}$ have been investigated because of their narrow bandgaps. Also, bandgaps of semiconductors have been engineered so that the light-harvesting properties are improved. [13]

Other than modifying the capability of light absorption, a construction of heterojunction is also considered as an effective strategy to improve efficiency because heterojunction semiconductors can enhance charge separation.^[14] When two materials are coupled, an internal electric field is typically created at the

junction. Many studies have reported that the induced electric field at the interface can promote charge separation by driving electron–hole pairs to transport in opposite directions and leading to a lower recombination rate. [15–20] For instance, Zhang et al. demonstrated that the PEC water-splitting efficiency of the WO₃/Cu₂O heterojunction photoelectrode significantly increased by 3.51 times that of a single WO₃ photoanode. [21]

Despite many strategies offering PEC efficiency improvement, the key to success is qualities and morphologies of photoelectrodes because these factors critically influence the performance of the system. [22] Chae et al. demonstrated that the morphological modification of the WO₃/BiVO₄ heterojunction film electrode can result in the enhancement of optical absorption ability, charge separation efficiency, and numbers of active sites for reaction, which facilitated the PEC processes and could reach a higher photocurrent density. [23] Some previous studies also emphasize that the interfacial quality of heterojunction is a crucial factor limiting the performance. [23–25] To obtain desirable electrode qualities, process optimization becomes essential. For example, Zhang et al. have presented that the morphology of WO₃/Sb₂S₃ heterojunction photocatalysts was pH-dependent, and by adjusting pH during the synthesis, the PEC watersplitting activity could be effectively enhanced. [26] Previous studies clearly show that the desirable morphology and film quality can simply be modified by varying synthesis parameters, such as growth and annealing temperatures. [27-30]

Among all heterojunction systems, a WO₃/BiVO₄ photoelectrode has the potential to be one of the efficient PEC systems due to the suitable band edge positions, the excellent visible-light response, and efficient charge separation.[17,25,31] Herein, we investigate the PEC performance of WO₃/BiVO₄ heterojunction thin-film photoanodes and the optimization of thermal treatment processes, namely preannealing and annealing steps for the improvement of PEC performance. The WO₃/BiVO₄ heterojunction thin films were prepared by a spin-coating method and then four conditions of thermal treatment processes were studied: 1) annealing for 0.5 h (W-BVO(NA, 400-0.5)), 2) preannealing followed by annealing for 0.5 h (W-BVO(A, 400-0.5)), 3) annealing for 5 h (W-BVO(NA, 400-5)), and 4) preannealing followed by annealing for 5 h (W-BVO(A, 400-5)). The effects of various thermal treatment conditions on photoelectrode properties were determined. The structure and morphology of the films were investigated by an X-ray diffractometer and a scanning electron microscope, respectively. Optical properties were also studied by UV-vis spectroscopy. Moreover, the PEC performances of all films were conducted and compared with a single-layered BiVO₄ photoelectrode. The results of this study could emphasize the significance of process parameters to tailor the PEC performance. In addition, it could provide vital information to design an efficient WO₃/BiVO₄ heterojunction as well as offer a strategy to improve PEC performance for clean hydrogen production.

2. Results and Discussion

2.1. Crystal Structures of WO₃/BiVO₄ Photoanodes

Phase formation of the $WO_3/BiVO_4$ heterojunction photoanodes prepared by spin coating the precursor solutions onto

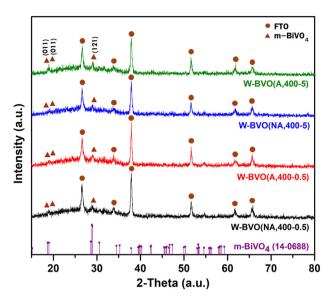


Figure 1. XRD patterns of the WO₃/BiVO₄ heterojunction thin-film photoanodes synthesized with different thermal treatment conditions.

fluorine-doped tin oxide (FTO) substrates with different thermal treatment conditions was characterized using an X-ray diffractometer. **Figure 1** shows the X-ray diffraction (XRD) patterns of all prepared photoanodes. The diffraction patterns exhibited peaks at 18.9°, 19.0°, and 28.9° which can be indexed to the (101), (011), and (121) planes of a monoclinic scheelite BiVO₄ phase (JCPDF no.14-0688). The other peaks belonged to the FTO substrate denoted with circle symbols. Also, it should be noted that the diffraction pattern of the WO₃ layers could not be clearly observed. This is possibly due to the crystallinity of the WO₃ layer. It is likely that the WO₃ layer possesses an amorphous structure. Hence, to verify the formation of the WO₃ layer, energy dispersive X-ray spectroscopy (EDS) was used. The EDS results (shown in Figure S1, Supporting Information) indicated a chemical composition of W and O, confirming the existence of the WO₃ layer.

In addition to the phase formation analyses, the full width at half maximum (FWHM) and the crystalline size were calculated based on the diffraction peak at 28.9°. The measured FWHM and the calculated crystalline size of all samples are shown in Table S2, Supporting Information. The results showed that the (W-BVO(A, 400-0.5)) and (W-BVO(A, 400-5)) samples had comparable crystallite sizes. Similarly, the crystallite sizes of the (W-BVO(NA, 400-0.5)) and (W-BVO(NA, 400-5)) samples were also comparable. This indicates that comparable crystallite sizes could be obtained when similar thermal treatment processes were programmed. Surprisingly, only the preannealing step was found to be significant on a crystalline size. In other words, the samples with the preannealing step had a much larger crystalline size than the samples without the preannealing step, whereas annealing the samples for a longer time did not cause much change in crystallite sizes. As a result, the preannealing process could be used to tailor the film crystallites as it strongly influences the crystallite size.

The morphologies of WO₃/BiVO₄ heterojunction thin-film photoanodes were investigated by scanning electron microscopy

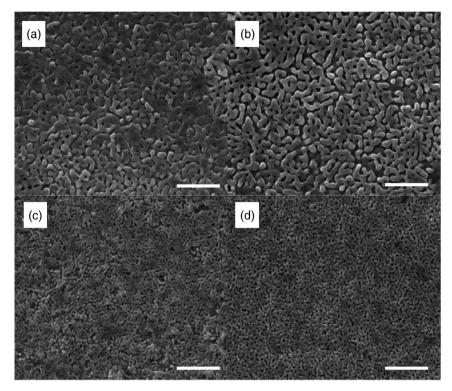


Figure 2. SEM images of the $WO_3/BiVO_4$ heterojunction thin-film photoanodes prepared under different thermal treatment conditions: a) W-BVO(NA, 400-5), b) W-BVO(A, 400-5), c) W-BVO(NA, 400-0.5), and d) W-BVO(A, 400-0.5). The scale bar represents 1 μ m in length.

(SEM). From the top-view images, the morphologies shown in Figure 2 demonstrated that all films possessed a network structure. Specifically, particles were all connected, but still there were pores between interconnected particles. Under different thermal treatment conditions, the dimension of the interconnected structure was altered. Increasing annealing time can widen the spacing of the interconnected structure. As a result, the films with longer annealing revealed a larger width of the network structure. [29,33] Moreover, compared with non-preannealed samples, the preannealed films were less dense and possessed a better uniformity with evenly distributed pores and spacing. This higher porosity and better uniformity may be attributed to a gradual evaporation of a precursor solution during a preannealing process. [34] This implies that an addition of preannealing could provide a better quality of films.

The preannealing process not only affect the morphology of the films, but also thicknesses of the films. Cross-sectional SEM analyses of the samples shown in Figure S3, Supporting Information, reveal the thickness of the films and the results are shown in Table S2, Supporting Information. The cross section of the samples demonstrated layers of FTO, WO₃, and BiVO₄. The films without the preannealing step showed comparable thicknesses even though they underwent the annealing step for different durations. This result is similar to the crystalline size analyses. Also, when adding the preannealing treatment, the film thicknesses relatively decreased. The decrease in thickness is possibly due to an evaporation of the precursor, causing the shrinkage of the film during preannealing.^[35]

2.2. Optical Properties

The optical properties of the $WO_3/BiVO_4$ heterojunction thinfilm photoanodes investigated by a UV–vis spectrophotometer are shown in **Figure 3**. The optical absorption behaviors determine the capability of the electrode to generate charge carriers. All samples exhibited a strong absorption within a range of 430–480 nm, with an absorption edge at \approx 480 nm, as shown in Figure 3a. However, the samples with preannealing showed an improved absorption ability. This could be explained by the high uniformity and crystallinity of the films. [36] Moreover, this finding also implies that controlling quality of films, specifically uniformity and crystallinity, could significantly improve optical properties.

Figure 3b shows the Tauc plot of the $WO_3/BiVO_4$ heterojunction photoanodes which is used to determine the bandgaps of the samples. The optical bandgaps of all photoanodes are calculated by Equation (1), and the results are shown in Table S2, Supporting Information.

$$(\alpha h v)^2 = h v - E_g \tag{1}$$

where $h\nu$ is an incident photon's energy (eV), $E_{\rm g}$ is an optical bandgap (eV), and α is the measured absorption coefficient.

From the Tauc plot (Figure 3b), the bandgap values of the samples were slightly different, and they were reduced with increasing the annealing time. This observation is in good agreement with previous studies.^[37] The shift to lower bandgap

800

Figure 3. a) UV-vis absorption spectra and b) Tauc plot of WO₃/BiVO₄ heterojunction thin-film photoanodes.

700

600

Wavelength (nm)

values with increasing annealing time may be attributed to more defect population formed due to the annealing process. It should be noted that the bandgap values determined from the estimation were between the bandgaps of $BiVO_4$ (2.4 eV)^[38] and WO_3 (2.7 eV).^[39] which is a property of the composite structure.

500

2.3. PEC Performance of WO₃/BiVO₄ Photoanodes

400

The PEC performance of the photoanodes was investigated using a potentiostat equipped with a standard three-electrode system and an illumination of 100 W light-emitting diode (LED) light source and the result is shown in Figure 4. Figure 4a shows the linear sweep voltammetry (LSV) curve, and the obtained photocurrent density at 1.23 V versus reversible hydrogen electrode (RHE) in 0.5 M Na₂SO₄ solution was 0.187, 0.054, 0.109, and $0.054 \,\mathrm{mA \, cm^{-2}}$ for W-BVO(A, 400-5), W-BVO(NA, 400-5), W-BVO(A, 400-0.5), and W-BVO(NA, 400-0.5), respectively. It should be noted that a preannealing treatment enhanced the photocurrent density. Plus, a longer annealing time could also further increase the performance. As a result, among all samples, W-BVO(A, 400-5) exhibited the best PEC performance. This result also corresponded to the onset potential, showing that the sample of W-BVO(A, 400-5) obtained the lowest value. This implies that the W-BVO(A, 400-5) sample requires the lowest potential to activate a water-splitting reaction. [40] More importantly, just by optimizing the thermal treatment parameters, the photocurrent density was increased by 3.46 times. In addition, compared with a single-layered BiVO₄ electrode, the onset potentials of the WO₃/BiVO₄ heterostructure electrode decreased. Such an onset potential reduction indicates that the heterostructure can promote kinetics of the reaction at the electrode surface enhancing the PEC performance.[41]

Figure 4b shows the comparison of the photocurrent density in the dark condition and under light irradiation. It is clear that the photocurrent density increased with the increase in voltage. Importantly, the photocurrent density under irradiation was higher than that in the dark condition. This result reveals that the samples are photoresponsive. In other words, when the samples were illuminated, electrons and holes were

generated, and the photocurrent density was increased. In addition, a time-dependent photocurrent response under the condition of chopped illumination is shown in Figure 4c. The result shows a noticeable spike of photocurrent density when the light was on. Then, a rapid decay in photocurrent density was observed before reaching a steady state. The spike could be related to an accumulation of charge carriers at the surface/electrolyte interface and then the reaction was suppressed by recombination, representing as rapid decay. Further, when the light was switched off, the photocurrent was back to zero. This behavior agrees well with the photoresponsiveness of the samples.^[42,43]

2.8

hυ (eV)

3.0

2.6

Water oxidation kinetics at the photoanode/electrolyte interface was also evaluated by the frequency response analyzer (FRA) impedance mode with a three-electrode system immersed in Na₂SO₄ electrolyte, and the result is shown in Figure 4d. Figure 4d shows the so-called Nyquist plots with an equivalent circuit shown in Figure 4e. It should be remarked that due to the different behaviors of the Nyquist plots, the equivalent circuit used for W-BVO(A, 400-5) is altered from the others. The FRA impedance analyses determined the charge transfer resistance (R_{ct}) at the interface between the WO₃/BiVO₄ heterojunction photoanodes and electrolytes. [44,45] The results revealed the R_{ct} values of 110.4, 4.2×10^3 , 11.7×10^3 , and $13.2 \times 10^3 \Omega$ for W-BVO(A- 400,5), W-BVO(NA- 400,5), W-BVO(A- 400,0.5) and W-BVO(NA- 400,0.5) photoanodes, respectively. Among all, the W-BVO (A-400,5) exhibited the smallest R_{ct} value which was in good agreement with its PEC performance. Due to its efficient charge transfer, the W-BVO(A-400,5) sample showed an improved PEC efficiency. These charge transfer resistance analyses also agree well with the applied bias photon-to-current conversion efficiency (ABPE) analyses, which are shown in Figure 5.

The ABPE values describe the photoresponse efficiency of a photoelectrode under an applied voltage. The ABPE values are a function of applied bias and can be calculated from the LSV curve using Equation (2).

ABPE(%) =
$$\frac{J_{i} \times (1.23 - E_{i})}{I_{light}} \times 100$$
 (2)

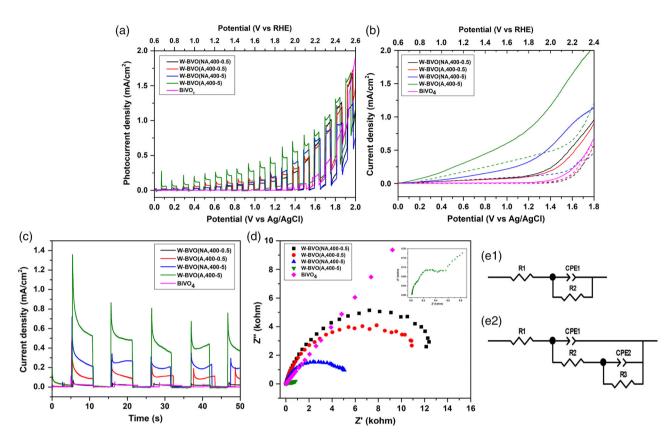


Figure 4. a) The LSV curve, b) the I-V curve comparison in the dark and light illumination, c) the chopped I-t curve at a constant applied potential of 1.23 V (vs Ag/AgCl), d) the Nyquist plots of WO₃/BiVO₄ heterojunction thin-film photoanodes in 0.5 M Na₂SO₄ electrolyte in 100 W LED illumination, (e1) the equivalent circuit for the W-BVO(NA, 400-5), W-BVO(A, 400-5), and W-BVO(NA, 400-0.5) photoelectrodes and (e2) the equivalent circuit for the W-BVO(A, 400-0.5) photoelectrode. In the equivalent circuit shown in Figure 4e1 and e2, R1 is the solution resistance (R_s), CPE1 is a constant phase element for the electrolyte/electrode interface, R2 is the charge transfer resistance across the interface of electrode/electrolyte (R_{ct}), and R3 is a capacitance and resistor of an absorbed layer (R_{ct2}).

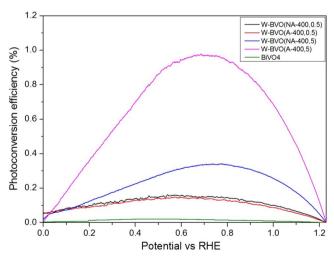
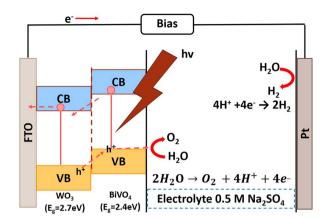


Figure 5. The ABPE of the $WO_3/BiVO_4$ heterojunction samples compared with a $BiVO_4$ photoelectrode.

where J_i is the measured photocurrent density at an applied voltage (mA cm⁻²); E_i is an applied voltage (V); and I_{light} is the light intensity (mW cm⁻²).

According to the ABPE curve, the samples with a longer annealing time provide better efficiencies. In addition, it clearly shows that all heterojunction samples have a much higher efficiency than a BiVO₄ photoanode. The higher efficiency in the heterojunction samples is potentially caused by the better charge separation due to an induced potential difference between WO₃ and BiVO₄. [46] Moreover, annealing the samples for a longer time could lead to robust film qualities, such as better interface. It is possible that a defect population at the interface was reduced by annealing for a certain time. This speculation could be further confirmed with more investigation, but it is not a focus of this study.

In general for photoanodes, after electrons and holes are generated, electrons will travel inward a semiconductor or toward an electron collector, whereas holes will travel toward an electrolyte. [47,48] As shown in **Scheme 1**, WO₃/BiVO₄ heterojunction consists of a band structure that could assist an electron–hole separation. [49] The conduction band and the valence band of the WO₃ layer are more positive than those of the BiVO₄ layer. Similarly, the valence band of the WO₃ layer is also more positive than that of the BiVO₄ layer. This band alignment is favorable for electrons to migrate toward the WO₃ layer and holes to travel outward the BiVO₄ electrolyte interface. [50,51]



Scheme 1. Schematic representation of the energy level and electron–hole transport in the $WO_3/BiVO_4$ heterojunction thin-film photoanodes of the PEC system.

The high PEC performance of the W-BVO(A,400-5) sample could also contribute to its film characteristics, including morphology and thickness. Specifically, high uniformity and high porosity of the interconnect-structured films are advantageous for photochemistry. These features provide a larger surface area for reaction sites, resulting in an increased photoactivity. ^[52] In addition, this film possessed the highest absorption ability, which could result in the largest population of photogenerated carriers as well as a higher possibility for charge carriers to reach the electrolyte/electrode interface, suggesting favorable attributes for a higher photocurrent density. ^[53–55] Therefore, by understanding the importance of parameters of thermal treatment, the process parameter can be optimized, and the efficient photoanode can be obtained.

3. Conclusions

In conclusion, we demonstrate that optimizing thermal treatment can improve the PEC performance. The thermal treatment strongly affected the structure and morphology of the WO₃/ BiVO₄ heterojunction thin-film photoanodes prepared by solution-based processing using a spin-coating technique followed by preannealing and annealing processes. The results showed that the preannealing treatment improved crystallinity, uniformity, and optical absorbance of the films, leading to an enhancement of the numbers of photogenerated charge carriers. With higher porosity, the preannealed films also obtained a larger interfacial area. The optimal thermal treatment was preannealing at 60 °C for 15 min, followed by calcining at 400 °C for 5 h. The photoanode with such an optimal treatment exhibited the highest photocurrent density under LED illumination. The WO₃/BiVO₄ heterojunction thin-film photoanodes also showed a better PEC performance than BiVO₄ photoanode due to an improved charge separation of the heterostructure. This study suggests a simple method to achieve the improvement of photoanode qualities as well as the PEC performance by optimizing thermal treatment conditions.

4. Experimental Section

Preparation of WO $_3$ Layers: A WO $_3$ layer was obtained by spin-coating processes. First, a precursor solution was prepared by dissolving tungstic acid (H $_2$ WO $_4$, Sigma-Aldrich, 6 mmol) into 1 M sulfuric acid (H $_2$ SO $_4$, 98% purity, ACI labscan, 6 mL) and was stirred for 24 h until the solution was homogeneous. Then, 27% hydrogen peroxide (H $_2$ O $_2$, Alfa Aesar) was added to obtain a clear solution. After that, the WO $_3$ precursor (200 µL) was dropped onto the FTO glass substrates (1 × 1.5 cm 2) for two-step spin-coating deposition. The processing parameters for spin coating were set as follows: the first speed was at 750 rpm for 10 s, and the second speed was at 3000 rpm for 25 s. The spin-coating process was repeated two times. Finally, the films were calcined at 550 °C for 2 h with a heating rate of 10 °C min $^{-1}$.

Preparation of WO₃/BiVO₄ Heterojunction Thin-Film Photoanodes: The WO₃/BiVO₄ photoanodes were prepared by spin coating BiVO₄ layers onto the predeposited WO₃ layer. For BiVO₄ deposition, a precursor prepared by dissolving ammonium metavanadate (NH₄VO₃, Daejung, 3 mmol) into 4 M nitric acid (HNO₃, 65% purity, Emsure, 10 mL). When the solution was stirred, bismuth nitrate pentahydrate (Bi(NO₃)₃.5H₂O, Daejung, 3 mmol) was added into the solution. After 3 h of stirring, the solution became yellowish. Then, citric acid (C₆H₈O₇, 6 mmol) was added into the solution and stirred until the solution turned blue. The blue solution (6 mL) was then mixed with polyvinyl alcohol solution (2 mL). This BiVO₄ precursor solution was used for spin-coating processes. The mixture (200 µL) was dropped onto an FTO substrate with the prepared WO₃ layer. The spin was set at the first speed of 750 rpm for 10 s and the second speed of 4000 rpm for 25 s.

After deposition, thermal treatment was conducted. To study the effect of thermal treatment on the films' performance, two steps for thermal treatment were varied: preannealing and annealing processes. The variables were the addition of a preannealing step and annealing time of 30 min and 5 h. Totally, four conditions were studied as denoted: W-BVO(NA, 400-0.5) was a sample with treatment condition of no preannealing treatment and annealing at 400 °C for 30 min; W-BVO(A, 400-0.5) was a sample with treatment condition of preannealing treatment at 60 °C for 15 min and annealing at 400 °C for 30 min; W-BVO(NA, 400-5) was a sample with treatment condition of no preannealing treatment and annealing at 400 °C for 5 h; and W-BVO(NA, 400-5) was a sample with the treatment condition of preannealing treatment at 60 °C for 15 min and annealing at 400 °C for 5 h.

Characterizations: The morphology of WO₃/BiVO₄ photoanodes was observed by SEM (FEI, Quanta450) equipped with an EDS used to analyze the film chemical composition. Phases of the samples were examined by XRD (Phillips X'pert) using Cu K α radiation ($\lambda = 1.5418$ Å). All patterns were recorded in the range of 15°–80° at a scan rate of 0.02° min⁻¹. The crystallite sizes of the samples were estimated using the Scherrer formula (Equation (3))

$$D = K\lambda/\beta\cos\theta\tag{3}$$

where D is the average crystallite size (nm), λ is the wavelength of X-ray radiation (0.15418 nm), K is the shape factor (0.9), [56] and β is the peak width at the half-maximum height (FWHM). The ultraviolet–visible spectrometer (UV-1700, Shimadzu) was used to measure the optical absorption of the prepared photoanodes (wavelength: 300–800 nm), and the optical bandgaps were calculated using the Tauc equation.

PEC Measurement: PEC measurement was carried out by potentiostat/galvanostats (Autolab PGSTAT 302N) using a three-electrode system. The WO $_3$ /BiVO $_4$ photoanodes were used as a working electrode, Pt was used as a counter electrode, and Ag/AgCl and saturated KCl electrode was used as a reference electrode. In addition, an aqueous solution containing 0.5 M Na $_2$ SO $_4$ was used as an electrolyte. LSV was conducted to examine PEC performance of the WO $_3$ /BiVO $_4$ photoanodes. For the measurement, the applied voltage was varied from -0.2 to $2.0\,\text{V}$ (vs Ag/AgCl) at a scanning rate of $10\,\text{mV}\,\text{s}^{-1}$. Also, a $100\,\text{W}$ LED was illuminated during the measurement. All reported potentials were calculated versus the RHE using Equation (4)

www.advancedsciencenews.com www.entechnol.de

$$E(vs RHE) = E(vs Ag/AgCl) + 0.05916 \times pH + 0.197(E^0 Ag/AgCl@room temp) = E(vs Ag/AgCl) + 0.05916 \times 7 + 0.197 = E(vs Ag/AgCl) + 0.611$$
(4)

The Nyquist plots were obtained using a potentiostat equipped with an FRA for impedance measurement. The potentiostat was conducted by applying an alternating current (AC) voltage with an amplitude of $-0.5\,\mathrm{V_{rms}}$ and the frequency varied from 10 kHz to 0.01 Hz in 0.5 M Na₂SO₄ solution under LED light illumination.^[57]

Supporting Information

Supporting Information is available from the Wiley Online Library or from the author.

Acknowledgements

This research received funding from Thailand Research Fund (MRG6180134), Faculty of Engineering, Kasetsart University. In addition, the authors gratefully acknowledge the facilities of Department of Materials Engineering, Faculty of Engineering, Kasetsart University.

Conflict of Interest

The authors declare no conflict of interest.

Keywords

photoanodes, photoelectrochemical performances, thermal treatments, WO3/BiVO4 heterojunctions

> Received: February 11, 2020 Revised: March 8, 2020 Published online:

- [1] K. Li, B. Lin, Renew. Sustainable Energy Rev. 2015, 52, 1107.
- [2] J. P. Holdren, Science 2007, 315, 737.
- [3] B. Parkinson, J. Turner, Energy and Environment Series (Eds: H.-J. Lewerenz, L. Peter), Royal Society of Chemistry, Cambridge 2013. 1.
- [4] D. K. Niakolas, M. Daletou, S. G. Neophytides, C. G. Vayenas, Ambio 2016, 45, 32.
- [5] I. Staffell, D. Scamman, A. V. Abad, P. Balcombe, P. E. Dodds, P. Ekins, N. Shah, K. R. Ward, Energy Environ. Sci. 2019, 12, 463.
- [6] A. Saeedmanesh, M. A. Mac Kinnon, J. Brouwer, Curr. Opin. Electrochem. 2018, 12, 166.
- [7] Z. Chen, H. Dinh, E. Miller, Photoelectrochemical Water Splitting: Standards, Experimental Methods, and Protocols, Springer-Verlag, New York, 2013.
- [8] O. Legrini, E. Oliveros, A. M. Braun, Chem. Rev. 1993, 93, 671.
- [9] K. C. Christoforidis, P. Fornasiero, ChemCatChem 2017, 9, 1523.
- [10] M. Heinemann, B. Eifert, C. Heiliger, Phys. Rev. B 2013, 87, 115111.
- [11] S. Piccinin, Phys. Chem. Chem. Phys. 2019, 21, 2957.
- [12] A. Walsh, Y. Yan, M. N. Huda, M. M. Al-Jassim, S.-H. Wei, Chem. Mater. 2009, 21, 547.
- [13] C. Wang, H. Qiu, T. Inoue, Q. Yao, Int. J. Hydrogen Energy 2014, 39, 12507.

- [14] S. J. A. Moniz, S. A. Shevlin, D. J. Martin, Z.-X. Guo, J. Tang, Energy Environ. Sci. 2015, 8, 731.
- [15] S. Bai, X. Yang, C. Liu, X. Xiang, R. Luo, J. He, A. Chen, ACS Sustainable Chem. Eng. 2018, 6, 12906.
- [16] K.-H. Ye, H. Li, D. Huang, S. Xiao, W. Qiu, M. Li, Y. Hu, W. Mai, H. Ji, S. Yang, Nat. Commun. 2019, 10, 1.
- [17] L. Zhang, M. Yang, Z. Luo, J. Zhang, Y. Hou, Int. J. Hydrogen Energy 2019. 44. 25652.
- [18] J. Sun, L. Sun, X. Yang, S. Bai, R. Luo, D. Li, A. Chen, Electrochim. Acta **2020**. *331*. 135282.
- [19] T. Zhang, J. Su, L. Guo, CrystEngComm 2016, 18, 8961.
- [20] Y. Pihosh, I. Turkevych, K. Mawatari, J. Uemura, Y. Kazoe, S. Kosar, K. Makita, T. Sugaya, T. Matsui, D. Fujita, M. Tosa, M. Kondo, T. Kitamori, Sci. Rep. 2015, 5, 11141.
- [21] J. Zhang, H. Ma, Z. Liu, Appl. Catal., B 2017, 201, 84.
- [22] W. Wang, M. Xu, X. Xu, W. Zhou, Z. Shao, Angew. Chem., Int. Ed. **2020**, 59, 136.
- [23] S. Y. Chae, C. S. Lee, H. Jung, O.-S. Joo, B. K. Min, J. H. Kim, Y. J. Hwang, ACS Appl. Mater. Interfaces 2017, 9, 19780.
- [24] T. Nakajima, T. Nakamura, T. Tsuchiya, Phys. Chem. Chem. Phys. 2014, 16, 26901.
- [25] B. S. Kalanoor, H. Seo, S. S. Kalanur, Mater. Sci. Energy Technol. 2018, 1, 49.
- [26] J. Zhang, Z. Liu, Z. Liu, ACS Appl. Mater. Interfaces 2016, 8, 9684.
- [27] Y.-S. Chen, L.-Y. Lin, Electrochim. Acta 2018, 285, 164.
- [28] S. Okunaka, Y. Hitomi, H. Tokudome, RSC Adv. 2018, 8, 31575.
- [29] S. Y. Jeong, K. S. Choi, H.-M. Shin, T. L. Kim, J. Song, S. Yoon, H. W. Jang, M.-H. Yoon, C. Jeon, J. Lee, S. Lee, ACS Appl. Mater. Interfaces 2017. 9. 505.
- [30] S. Hilliard, D. Friedrich, S. Kressman, H. Strub, V. Artero, C. Laberty-Robert, ChemPhotoChem 2017, 1, 273.
- [31] Q. Zeng, J. Li, L. Li, J. Bai, L. Xia, B. Zhou, Appl. Catal. B 2017, 217, 21.
- [32] S. M. Thalluri, C. Martinez Suarez, M. Hussain, S. Hernandez, A. Virga, G. Saracco, N. Russo, Ind. Eng. Chem. Res. 2013, 52, 17414.
- [33] X. Ren, Z. Yang, D. Yang, X. Zhang, D. Cui, Y. Liu, Q. Wei, H. Fan, S. (Frank) Liu, Nanoscale 2016, 8, 3816.
- [34] S. Okunaka, Y. Hitomi, H. Tokudome, RSC Adv. 2018, 8, 31575.
- [35] L. Shi, S. Zhuo, M. Abulikemu, G. Mettela, T. Palaniselvam, S. Rasul, B. Tang, B. Yan, N. B. Saleh, P. Wang, RSC Adv. 2018, 8, 29179.
- [36] F. F. Abdi, L. Han, A. H. M. Smets, M. Zeman, B. Dam, R. van de Krol, Nat. Commun. 2013, 4, 2195.
- [37] J. K. Cooper, S. Gul, F. M. Toma, L. Chen, Y.-S. Liu, J. Guo, J. W. Ager, J. Yano, I. D. Sharp, J. Phys. Chem. C 2015, 119, 2969.
- [38] Z. Zhao, Z. Li, Z. Zou, Phys. Chem. Chem. Phys. 2011, 13, 4746.
- [39] P. P. González-Borrero, F. Sato, A. N. Medina, M. L. Baesso, A. C. Bento, G. Baldissera, C. Persson, G. A. Niklasson, C. G. Granqvist, A. Ferreira da Silva, Appl. Phys. Lett. 2010, 96, 061909.
- [40] H. He, S. P. Berglund, A. J. E. Rettie, W. D. Chemelewski, P. Xiao, Y. Zhang, C. B. Mullins, J. Mater. Chem. A 2014, 2, 9371.
- [41] R. Tang, S. Zhou, Z. Yuan, L. Yin, Adv. Funct. Mater. 2017, 27, 1701102.
- [42] X. Wan, F. Niu, J. Su, L. Guo, Phys. Chem. Chem. Phys. 2016, 18,
- [43] C. Zachäus, F. F. Abdi, L. M. Peter, R. van de Krol, Chem. Sci. 2017, 8,
- [44] Y. Huang, Y. Yu, Y. Xin, N. Meng, Y. Yu, B. Zhang, Sci. China Mater. 2017, 60, 193.
- [45] H. He, Y. Zhou, G. Ke, X. Zhong, M. Yang, L. Bian, K. Lv, F. Dong, Electrochim. Acta 2017, 257, 181.
- [46] K. Pingmuang, J. Chen, W. Kangwansupamonkon, G. G. Wallace, S. Phanichphant, A. Nattestad, Sci. Rep. 2017, 7, 8929.

www.entechnol.de



www.advancedsciencenews.com

- [47] F. F. Abdi, N. Firet, R. van de Krol, ChemCatChem 2013, 5, 490.
- [48] B.-C. Xiao, L.-Y. Lin, J.-Y. Hong, H.-S. Lin, Y.-T. Song, RSC Adv. 2017, *7*, 7547.
- [49] C. Martinez Suarez, S. Hernández, N. Russo, Appl. Catal. A 2015, *504*, 158.
- [50] H. W. Jeong, T. H. Jeon, J. S. Jang, W. Choi, H. Park, J. Phys. Chem. C **2013**, *117*, 9104.
- [51] J. H. Seo, G. Park, K. H. Oh, S. H. Kang, H. C. Lee, S. K. Cho, K. M. Nam, J. Electroanal. Chem. 2017, 789, 17.
- [52] L. Xia, J. Bai, J. Li, Q. Zeng, X. Li, B. Zhou, Appl. Catal. B 2016, 183, 224.
- [53] M. G. Lee, D. H. Kim, W. Sohn, C. W. Moon, H. Park, S. Lee, H. W. Jang, Nano Energy 2016, 28, 250.
- [54] S. J. Hong, S. Lee, J. S. Jang, J. S. Lee, Energy Environ. Sci. 2011, *4*, 1781.
- [55] S.-L. Chen, L.-Y. Lin, Y.-S. Chen, Electrochim. Acta 2019, 295, 507.
- [56] E. Warren Bertram, X-Ray Diffraction, Addison-Wesley Pub. Co, Reading, MA 1969.
- [57] T. M. Nahir, J. Am. Chem. Soc. 2005, 127, 12431.

The Improved Photoelectrochemical Performance of WO₃/BiVO₄ Heterojunction Thin-Film Photoanodes via Thermal Treatment

Soriya Phiankoh, Pongthep Prajongtat, Metta Chareonpanich, and Ratiporn Munprom*

Improvement in the photoelectrochemical (PEC) performance of WO₃/BiVO₄ heterojunction photoanodes is achieved by thermal treatment. The heterostructure systems consist of WO3 and BiVO4 layers spin coated onto fluorinedoped tin oxide (FTO)-coated glass substrates. The morphology and optical properties are modified by varying annealing conditions and calcining time. The crystal structure, morphology, and optical properties are studied using X-ray diffraction (XRD), scanning electron microscopy (SEM), and UV-vis spectroscopy, respectively. The results show that the WO₃/BiVO₄ photoanodes obtain an interconnected structure which helps promote the PEC activity by increasing the active area for reaction and shortening the distance for carrier diffusion. Also, the preannealing treatment can improve film qualities, namely crystallinity, uniformity, and optical absorbance, leading to an enhancement of the PEC performance. The optimal thermal treatment is preannealing at 60 °C for 15 min, followed by calcining at 400 °C for 5 h. The photoanode with such an optimal treatment exhibits the highest photocurrent density under light-emitting diode (LED) illumination, and the efficiency is increased by 3-4 times compared with the others. Herein, a simple method is offered to improve the PEC performance of a heterojunction photoelectrode.

1. Introduction

An energy insufficiency is one of the global issues that may be encountered in the future. With the rapid development of

S. Phiankoh, Dr. R. Munprom Department of Materials Engineering Faculty of Engineering Kasetsart University

50 Ngamwongwan Rd., Chatuchak, Bangkok 10900, Thailand E-mail: fengrtpm@ku.ac.th Dr. P. Prajongtat

Department of Materials Science Faculty of Science Kasetsart University 50 Ngamwongwan Rd., Chatuchak, Bangkok 10900, Thailand Prof. M. Chareonpanich Department of Chemical Engineering Faculty of Engineering Kasetsart University 50 Ngamwongwan Rd., Chatuchak, Bangkok 10900, Thailand

The ORCID identification number(s) for the author(s) of this article can be found under https://doi.org/10.1002/ente.202000147.

DOI: 10.1002/ente.202000147

industrialization and an increase in population driving to expansion in energy needs, this problem becomes more severe and it may come sooner than expected. [1,2] Therefore, it is necessary to find alternative energy sources to substitute the current use of limited fossil fuels.[3] The requirements of alternative energy that should be considered are cleanliness, affordability, harvesting/conversion efficiency, and sustainability.[4]

Hydrogen is considered as one of our hopes for alternative fuels. Hydrogen is an abundant element and can be found in many organic compounds, such as water and petrochemicals. Moreover, hydrogen fuel contains the highest energy density per mass. One kilogram of hydrogen fuel can produce $\approx 120 \,\mathrm{MJ}$ energy, which is three times higher than energy produced from the equivalent amount of gasoline.^[5] More importantly, its combustion is zero emission which makes hydrogen gas attractive as an efficient and clean fuel.[6]

Photoelectrochemical (PEC) water splitting is a technology to produce hydrogen fuel. The system utilizes semiconductor photoelectrodes and solar energy to convert water to hydrogen fuel. This energy conversion becomes one of the widely studied research areas because it can sustainably supply clean chemical energy. [7-9] The conversion process involves three crucial steps that can limit efficiency: 1) electron-hole generation, 2) electron-hole separation, and 3) electron-hole utilization. Many researchers are intensively attempting to improve the overall photoelectrochemical (PEC) performance by simply improving efficiencies of the three steps in the process. Research works have profoundly been devoted to developing novel photoelectrodes with excellent light-absorbing ability, aimed to enhance electron-hole generation. For example, many visible-light responsive oxides, such as Cu_2O ($E_g=2.17\,\text{eV}$), $^{[10]}$ Fe_2O_3 ($E_g=2.2\,\text{eV}$), $^{[11]}$ and BiVO_4 ($E_g=2.4\,\text{eV}$), $^{[12]}$ have been investigated because of their narrow bandgaps. Also, bandgaps of semiconductors have been engineered so that the light-harvesting properties are improved. [13]

Other than modifying the capability of light absorption, a construction of heterojunction is also considered as an effective strategy to improve efficiency because heterojunction semiconductors can enhance charge separation.^[14] When two materials are coupled, an internal electric field is typically created at the

junction. Many studies have reported that the induced electric field at the interface can promote charge separation by driving electron–hole pairs to transport in opposite directions and leading to a lower recombination rate. [15–20] For instance, Zhang et al. demonstrated that the PEC water-splitting efficiency of the WO₃/Cu₂O heterojunction photoelectrode significantly increased by 3.51 times that of a single WO₃ photoanode. [21]

Despite many strategies offering PEC efficiency improvement, the key to success is qualities and morphologies of photoelectrodes because these factors critically influence the performance of the system. [22] Chae et al. demonstrated that the morphological modification of the WO₃/BiVO₄ heterojunction film electrode can result in the enhancement of optical absorption ability, charge separation efficiency, and numbers of active sites for reaction, which facilitated the PEC processes and could reach a higher photocurrent density. [23] Some previous studies also emphasize that the interfacial quality of heterojunction is a crucial factor limiting the performance. [23–25] To obtain desirable electrode qualities, process optimization becomes essential. For example, Zhang et al. have presented that the morphology of WO₃/Sb₂S₃ heterojunction photocatalysts was pH-dependent, and by adjusting pH during the synthesis, the PEC watersplitting activity could be effectively enhanced. [26] Previous studies clearly show that the desirable morphology and film quality can simply be modified by varying synthesis parameters, such as growth and annealing temperatures. [27-30]

Among all heterojunction systems, a WO₃/BiVO₄ photoelectrode has the potential to be one of the efficient PEC systems due to the suitable band edge positions, the excellent visible-light response, and efficient charge separation.[17,25,31] Herein, we investigate the PEC performance of WO₃/BiVO₄ heterojunction thin-film photoanodes and the optimization of thermal treatment processes, namely preannealing and annealing steps for the improvement of PEC performance. The WO₃/BiVO₄ heterojunction thin films were prepared by a spin-coating method and then four conditions of thermal treatment processes were studied: 1) annealing for 0.5 h (W-BVO(NA, 400-0.5)), 2) preannealing followed by annealing for 0.5 h (W-BVO(A, 400-0.5)), 3) annealing for 5 h (W-BVO(NA, 400-5)), and 4) preannealing followed by annealing for 5 h (W-BVO(A, 400-5)). The effects of various thermal treatment conditions on photoelectrode properties were determined. The structure and morphology of the films were investigated by an X-ray diffractometer and a scanning electron microscope, respectively. Optical properties were also studied by UV-vis spectroscopy. Moreover, the PEC performances of all films were conducted and compared with a single-layered BiVO₄ photoelectrode. The results of this study could emphasize the significance of process parameters to tailor the PEC performance. In addition, it could provide vital information to design an efficient WO₃/BiVO₄ heterojunction as well as offer a strategy to improve PEC performance for clean hydrogen production.

2. Results and Discussion

2.1. Crystal Structures of WO₃/BiVO₄ Photoanodes

Phase formation of the $WO_3/BiVO_4$ heterojunction photoanodes prepared by spin coating the precursor solutions onto

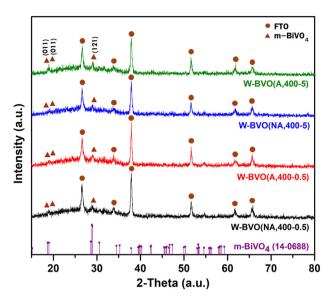


Figure 1. XRD patterns of the WO₃/BiVO₄ heterojunction thin-film photoanodes synthesized with different thermal treatment conditions.

fluorine-doped tin oxide (FTO) substrates with different thermal treatment conditions was characterized using an X-ray diffractometer. **Figure 1** shows the X-ray diffraction (XRD) patterns of all prepared photoanodes. The diffraction patterns exhibited peaks at 18.9°, 19.0°, and 28.9° which can be indexed to the (101), (011), and (121) planes of a monoclinic scheelite BiVO₄ phase (JCPDF no.14-0688). The other peaks belonged to the FTO substrate denoted with circle symbols. Also, it should be noted that the diffraction pattern of the WO₃ layers could not be clearly observed. This is possibly due to the crystallinity of the WO₃ layer. It is likely that the WO₃ layer possesses an amorphous structure. Hence, to verify the formation of the WO₃ layer, energy dispersive X-ray spectroscopy (EDS) was used. The EDS results (shown in Figure S1, Supporting Information) indicated a chemical composition of W and O, confirming the existence of the WO₃ layer.

In addition to the phase formation analyses, the full width at half maximum (FWHM) and the crystalline size were calculated based on the diffraction peak at 28.9°. The measured FWHM and the calculated crystalline size of all samples are shown in Table S2, Supporting Information. The results showed that the (W-BVO(A, 400-0.5)) and (W-BVO(A, 400-5)) samples had comparable crystallite sizes. Similarly, the crystallite sizes of the (W-BVO(NA, 400-0.5)) and (W-BVO(NA, 400-5)) samples were also comparable. This indicates that comparable crystallite sizes could be obtained when similar thermal treatment processes were programmed. Surprisingly, only the preannealing step was found to be significant on a crystalline size. In other words, the samples with the preannealing step had a much larger crystalline size than the samples without the preannealing step, whereas annealing the samples for a longer time did not cause much change in crystallite sizes. As a result, the preannealing process could be used to tailor the film crystallites as it strongly influences the crystallite size.

The morphologies of WO₃/BiVO₄ heterojunction thin-film photoanodes were investigated by scanning electron microscopy

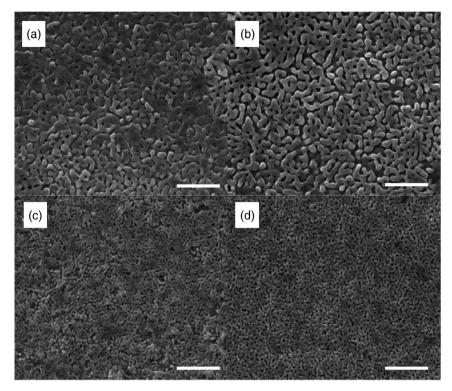


Figure 2. SEM images of the $WO_3/BiVO_4$ heterojunction thin-film photoanodes prepared under different thermal treatment conditions: a) W-BVO(NA, 400-5), b) W-BVO(A, 400-5), c) W-BVO(NA, 400-0.5), and d) W-BVO(A, 400-0.5). The scale bar represents 1 μ m in length.

(SEM). From the top-view images, the morphologies shown in Figure 2 demonstrated that all films possessed a network structure. Specifically, particles were all connected, but still there were pores between interconnected particles. Under different thermal treatment conditions, the dimension of the interconnected structure was altered. Increasing annealing time can widen the spacing of the interconnected structure. As a result, the films with longer annealing revealed a larger width of the network structure. [29,33] Moreover, compared with non-preannealed samples, the preannealed films were less dense and possessed a better uniformity with evenly distributed pores and spacing. This higher porosity and better uniformity may be attributed to a gradual evaporation of a precursor solution during a preannealing process. [34] This implies that an addition of preannealing could provide a better quality of films.

The preannealing process not only affect the morphology of the films, but also thicknesses of the films. Cross-sectional SEM analyses of the samples shown in Figure S3, Supporting Information, reveal the thickness of the films and the results are shown in Table S2, Supporting Information. The cross section of the samples demonstrated layers of FTO, WO₃, and BiVO₄. The films without the preannealing step showed comparable thicknesses even though they underwent the annealing step for different durations. This result is similar to the crystalline size analyses. Also, when adding the preannealing treatment, the film thicknesses relatively decreased. The decrease in thickness is possibly due to an evaporation of the precursor, causing the shrinkage of the film during preannealing.^[35]

2.2. Optical Properties

The optical properties of the $WO_3/BiVO_4$ heterojunction thinfilm photoanodes investigated by a UV–vis spectrophotometer are shown in **Figure 3**. The optical absorption behaviors determine the capability of the electrode to generate charge carriers. All samples exhibited a strong absorption within a range of 430–480 nm, with an absorption edge at \approx 480 nm, as shown in Figure 3a. However, the samples with preannealing showed an improved absorption ability. This could be explained by the high uniformity and crystallinity of the films. [36] Moreover, this finding also implies that controlling quality of films, specifically uniformity and crystallinity, could significantly improve optical properties.

Figure 3b shows the Tauc plot of the $WO_3/BiVO_4$ heterojunction photoanodes which is used to determine the bandgaps of the samples. The optical bandgaps of all photoanodes are calculated by Equation (1), and the results are shown in Table S2, Supporting Information.

$$(\alpha h v)^2 = h v - E_g \tag{1}$$

where $h\nu$ is an incident photon's energy (eV), $E_{\rm g}$ is an optical bandgap (eV), and α is the measured absorption coefficient.

From the Tauc plot (Figure 3b), the bandgap values of the samples were slightly different, and they were reduced with increasing the annealing time. This observation is in good agreement with previous studies.^[37] The shift to lower bandgap

800

Figure 3. a) UV-vis absorption spectra and b) Tauc plot of WO₃/BiVO₄ heterojunction thin-film photoanodes.

700

600

Wavelength (nm)

values with increasing annealing time may be attributed to more defect population formed due to the annealing process. It should be noted that the bandgap values determined from the estimation were between the bandgaps of $BiVO_4$ (2.4 eV)^[38] and WO_3 (2.7 eV).^[39] which is a property of the composite structure.

500

2.3. PEC Performance of WO₃/BiVO₄ Photoanodes

400

The PEC performance of the photoanodes was investigated using a potentiostat equipped with a standard three-electrode system and an illumination of 100 W light-emitting diode (LED) light source and the result is shown in Figure 4. Figure 4a shows the linear sweep voltammetry (LSV) curve, and the obtained photocurrent density at 1.23 V versus reversible hydrogen electrode (RHE) in 0.5 M Na₂SO₄ solution was 0.187, 0.054, 0.109, and $0.054 \,\mathrm{mA \, cm^{-2}}$ for W-BVO(A, 400-5), W-BVO(NA, 400-5), W-BVO(A, 400-0.5), and W-BVO(NA, 400-0.5), respectively. It should be noted that a preannealing treatment enhanced the photocurrent density. Plus, a longer annealing time could also further increase the performance. As a result, among all samples, W-BVO(A, 400-5) exhibited the best PEC performance. This result also corresponded to the onset potential, showing that the sample of W-BVO(A, 400-5) obtained the lowest value. This implies that the W-BVO(A, 400-5) sample requires the lowest potential to activate a water-splitting reaction. [40] More importantly, just by optimizing the thermal treatment parameters, the photocurrent density was increased by 3.46 times. In addition, compared with a single-layered BiVO₄ electrode, the onset potentials of the WO₃/BiVO₄ heterostructure electrode decreased. Such an onset potential reduction indicates that the heterostructure can promote kinetics of the reaction at the electrode surface enhancing the PEC performance.[41]

Figure 4b shows the comparison of the photocurrent density in the dark condition and under light irradiation. It is clear that the photocurrent density increased with the increase in voltage. Importantly, the photocurrent density under irradiation was higher than that in the dark condition. This result reveals that the samples are photoresponsive. In other words, when the samples were illuminated, electrons and holes were

generated, and the photocurrent density was increased. In addition, a time-dependent photocurrent response under the condition of chopped illumination is shown in Figure 4c. The result shows a noticeable spike of photocurrent density when the light was on. Then, a rapid decay in photocurrent density was observed before reaching a steady state. The spike could be related to an accumulation of charge carriers at the surface/electrolyte interface and then the reaction was suppressed by recombination, representing as rapid decay. Further, when the light was switched off, the photocurrent was back to zero. This behavior agrees well with the photoresponsiveness of the samples.^[42,43]

2.8

hυ (eV)

3.0

2.6

Water oxidation kinetics at the photoanode/electrolyte interface was also evaluated by the frequency response analyzer (FRA) impedance mode with a three-electrode system immersed in Na₂SO₄ electrolyte, and the result is shown in Figure 4d. Figure 4d shows the so-called Nyquist plots with an equivalent circuit shown in Figure 4e. It should be remarked that due to the different behaviors of the Nyquist plots, the equivalent circuit used for W-BVO(A, 400-5) is altered from the others. The FRA impedance analyses determined the charge transfer resistance (R_{ct}) at the interface between the WO₃/BiVO₄ heterojunction photoanodes and electrolytes. [44,45] The results revealed the R_{ct} values of 110.4, 4.2×10^3 , 11.7×10^3 , and $13.2 \times 10^3 \Omega$ for W-BVO(A- 400,5), W-BVO(NA- 400,5), W-BVO(A- 400,0.5) and W-BVO(NA- 400,0.5) photoanodes, respectively. Among all, the W-BVO (A-400,5) exhibited the smallest R_{ct} value which was in good agreement with its PEC performance. Due to its efficient charge transfer, the W-BVO(A-400,5) sample showed an improved PEC efficiency. These charge transfer resistance analyses also agree well with the applied bias photon-to-current conversion efficiency (ABPE) analyses, which are shown in Figure 5.

The ABPE values describe the photoresponse efficiency of a photoelectrode under an applied voltage. The ABPE values are a function of applied bias and can be calculated from the LSV curve using Equation (2).

ABPE(%) =
$$\frac{J_{i} \times (1.23 - E_{i})}{I_{light}} \times 100$$
 (2)

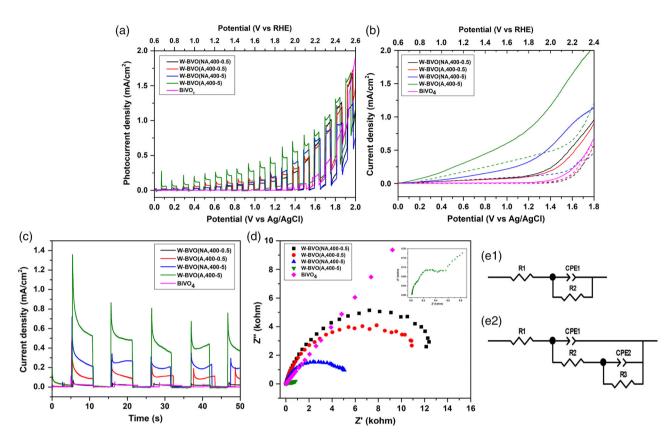


Figure 4. a) The LSV curve, b) the I-V curve comparison in the dark and light illumination, c) the chopped I-t curve at a constant applied potential of 1.23 V (vs Ag/AgCl), d) the Nyquist plots of WO₃/BiVO₄ heterojunction thin-film photoanodes in 0.5 M Na₂SO₄ electrolyte in 100 W LED illumination, (e1) the equivalent circuit for the W-BVO(NA, 400-5), W-BVO(A, 400-5), and W-BVO(NA, 400-0.5) photoelectrodes and (e2) the equivalent circuit for the W-BVO(A, 400-0.5) photoelectrode. In the equivalent circuit shown in Figure 4e1 and e2, R1 is the solution resistance (R_s), CPE1 is a constant phase element for the electrolyte/electrode interface, R2 is the charge transfer resistance across the interface of electrode/electrolyte (R_{ct}), and R3 is a capacitance and resistor of an absorbed layer (R_{ct2}).

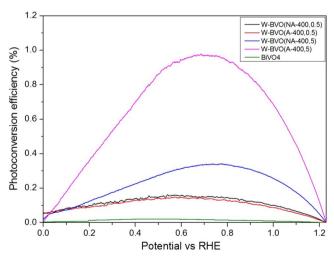
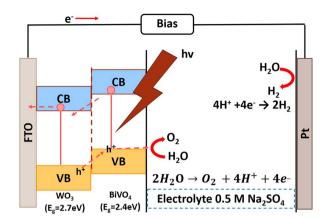


Figure 5. The ABPE of the $WO_3/BiVO_4$ heterojunction samples compared with a $BiVO_4$ photoelectrode.

where J_i is the measured photocurrent density at an applied voltage (mA cm⁻²); E_i is an applied voltage (V); and I_{light} is the light intensity (mW cm⁻²).

According to the ABPE curve, the samples with a longer annealing time provide better efficiencies. In addition, it clearly shows that all heterojunction samples have a much higher efficiency than a BiVO₄ photoanode. The higher efficiency in the heterojunction samples is potentially caused by the better charge separation due to an induced potential difference between WO₃ and BiVO₄. [46] Moreover, annealing the samples for a longer time could lead to robust film qualities, such as better interface. It is possible that a defect population at the interface was reduced by annealing for a certain time. This speculation could be further confirmed with more investigation, but it is not a focus of this study.

In general for photoanodes, after electrons and holes are generated, electrons will travel inward a semiconductor or toward an electron collector, whereas holes will travel toward an electrolyte. [47,48] As shown in **Scheme 1**, WO₃/BiVO₄ heterojunction consists of a band structure that could assist an electron–hole separation. [49] The conduction band and the valence band of the WO₃ layer are more positive than those of the BiVO₄ layer. Similarly, the valence band of the WO₃ layer is also more positive than that of the BiVO₄ layer. This band alignment is favorable for electrons to migrate toward the WO₃ layer and holes to travel outward the BiVO₄ electrolyte interface. [50,51]



Scheme 1. Schematic representation of the energy level and electron–hole transport in the $WO_3/BiVO_4$ heterojunction thin-film photoanodes of the PEC system.

The high PEC performance of the W-BVO(A,400-5) sample could also contribute to its film characteristics, including morphology and thickness. Specifically, high uniformity and high porosity of the interconnect-structured films are advantageous for photochemistry. These features provide a larger surface area for reaction sites, resulting in an increased photoactivity. ^[52] In addition, this film possessed the highest absorption ability, which could result in the largest population of photogenerated carriers as well as a higher possibility for charge carriers to reach the electrolyte/electrode interface, suggesting favorable attributes for a higher photocurrent density. ^[53–55] Therefore, by understanding the importance of parameters of thermal treatment, the process parameter can be optimized, and the efficient photoanode can be obtained.

3. Conclusions

In conclusion, we demonstrate that optimizing thermal treatment can improve the PEC performance. The thermal treatment strongly affected the structure and morphology of the WO₃/ BiVO₄ heterojunction thin-film photoanodes prepared by solution-based processing using a spin-coating technique followed by preannealing and annealing processes. The results showed that the preannealing treatment improved crystallinity, uniformity, and optical absorbance of the films, leading to an enhancement of the numbers of photogenerated charge carriers. With higher porosity, the preannealed films also obtained a larger interfacial area. The optimal thermal treatment was preannealing at 60 °C for 15 min, followed by calcining at 400 °C for 5 h. The photoanode with such an optimal treatment exhibited the highest photocurrent density under LED illumination. The WO₃/BiVO₄ heterojunction thin-film photoanodes also showed a better PEC performance than BiVO₄ photoanode due to an improved charge separation of the heterostructure. This study suggests a simple method to achieve the improvement of photoanode qualities as well as the PEC performance by optimizing thermal treatment conditions.

4. Experimental Section

Preparation of WO $_3$ Layers: A WO $_3$ layer was obtained by spin-coating processes. First, a precursor solution was prepared by dissolving tungstic acid (H $_2$ WO $_4$, Sigma-Aldrich, 6 mmol) into 1 M sulfuric acid (H $_2$ SO $_4$, 98% purity, ACI labscan, 6 mL) and was stirred for 24 h until the solution was homogeneous. Then, 27% hydrogen peroxide (H $_2$ O $_2$, Alfa Aesar) was added to obtain a clear solution. After that, the WO $_3$ precursor (200 µL) was dropped onto the FTO glass substrates (1 × 1.5 cm 2) for two-step spin-coating deposition. The processing parameters for spin coating were set as follows: the first speed was at 750 rpm for 10 s, and the second speed was at 3000 rpm for 25 s. The spin-coating process was repeated two times. Finally, the films were calcined at 550 °C for 2 h with a heating rate of 10 °C min $^{-1}$.

Preparation of WO₃/BiVO₄ Heterojunction Thin-Film Photoanodes: The WO₃/BiVO₄ photoanodes were prepared by spin coating BiVO₄ layers onto the predeposited WO₃ layer. For BiVO₄ deposition, a precursor prepared by dissolving ammonium metavanadate (NH₄VO₃, Daejung, 3 mmol) into 4 M nitric acid (HNO₃, 65% purity, Emsure, 10 mL). When the solution was stirred, bismuth nitrate pentahydrate (Bi(NO₃)₃.5H₂O, Daejung, 3 mmol) was added into the solution. After 3 h of stirring, the solution became yellowish. Then, citric acid (C₆H₈O₇, 6 mmol) was added into the solution and stirred until the solution turned blue. The blue solution (6 mL) was then mixed with polyvinyl alcohol solution (2 mL). This BiVO₄ precursor solution was used for spin-coating processes. The mixture (200 µL) was dropped onto an FTO substrate with the prepared WO₃ layer. The spin was set at the first speed of 750 rpm for 10 s and the second speed of 4000 rpm for 25 s.

After deposition, thermal treatment was conducted. To study the effect of thermal treatment on the films' performance, two steps for thermal treatment were varied: preannealing and annealing processes. The variables were the addition of a preannealing step and annealing time of 30 min and 5 h. Totally, four conditions were studied as denoted: W-BVO(NA, 400-0.5) was a sample with treatment condition of no preannealing treatment and annealing at 400 °C for 30 min; W-BVO(A, 400-0.5) was a sample with treatment condition of preannealing treatment at 60 °C for 15 min and annealing at 400 °C for 30 min; W-BVO(NA, 400-5) was a sample with treatment condition of no preannealing treatment and annealing at 400 °C for 5 h; and W-BVO(NA, 400-5) was a sample with the treatment condition of preannealing treatment at 60 °C for 15 min and annealing at 400 °C for 5 h.

Characterizations: The morphology of WO₃/BiVO₄ photoanodes was observed by SEM (FEI, Quanta450) equipped with an EDS used to analyze the film chemical composition. Phases of the samples were examined by XRD (Phillips X'pert) using Cu K α radiation ($\lambda = 1.5418$ Å). All patterns were recorded in the range of 15°–80° at a scan rate of 0.02° min⁻¹. The crystallite sizes of the samples were estimated using the Scherrer formula (Equation (3))

$$D = K\lambda/\beta\cos\theta\tag{3}$$

where D is the average crystallite size (nm), λ is the wavelength of X-ray radiation (0.15418 nm), K is the shape factor (0.9), [56] and β is the peak width at the half-maximum height (FWHM). The ultraviolet–visible spectrometer (UV-1700, Shimadzu) was used to measure the optical absorption of the prepared photoanodes (wavelength: 300–800 nm), and the optical bandgaps were calculated using the Tauc equation.

PEC Measurement: PEC measurement was carried out by potentiostat/galvanostats (Autolab PGSTAT 302N) using a three-electrode system. The WO $_3$ /BiVO $_4$ photoanodes were used as a working electrode, Pt was used as a counter electrode, and Ag/AgCl and saturated KCl electrode was used as a reference electrode. In addition, an aqueous solution containing 0.5 M Na $_2$ SO $_4$ was used as an electrolyte. LSV was conducted to examine PEC performance of the WO $_3$ /BiVO $_4$ photoanodes. For the measurement, the applied voltage was varied from -0.2 to $2.0\,\text{V}$ (vs Ag/AgCl) at a scanning rate of $10\,\text{mV}\,\text{s}^{-1}$. Also, a $100\,\text{W}$ LED was illuminated during the measurement. All reported potentials were calculated versus the RHE using Equation (4)

www.advancedsciencenews.com www.entechnol.de

$$E(vs RHE) = E(vs Ag/AgCl) + 0.05916 \times pH + 0.197(E^0 Ag/AgCl@room temp) = E(vs Ag/AgCl) + 0.05916 \times 7 + 0.197 = E(vs Ag/AgCl) + 0.611$$
(4)

The Nyquist plots were obtained using a potentiostat equipped with an FRA for impedance measurement. The potentiostat was conducted by applying an alternating current (AC) voltage with an amplitude of $-0.5\,\mathrm{V_{rms}}$ and the frequency varied from 10 kHz to 0.01 Hz in 0.5 M Na₂SO₄ solution under LED light illumination.^[57]

Supporting Information

Supporting Information is available from the Wiley Online Library or from the author.

Acknowledgements

This research received funding from Thailand Research Fund (MRG6180134), Faculty of Engineering, Kasetsart University. In addition, the authors gratefully acknowledge the facilities of Department of Materials Engineering, Faculty of Engineering, Kasetsart University.

Conflict of Interest

The authors declare no conflict of interest.

Keywords

photoanodes, photoelectrochemical performances, thermal treatments, WO3/BiVO4 heterojunctions

> Received: February 11, 2020 Revised: March 8, 2020 Published online:

- [1] K. Li, B. Lin, Renew. Sustainable Energy Rev. 2015, 52, 1107.
- [2] J. P. Holdren, Science 2007, 315, 737.
- [3] B. Parkinson, J. Turner, Energy and Environment Series (Eds: H.-J. Lewerenz, L. Peter), Royal Society of Chemistry, Cambridge 2013. 1.
- [4] D. K. Niakolas, M. Daletou, S. G. Neophytides, C. G. Vayenas, Ambio 2016, 45, 32.
- [5] I. Staffell, D. Scamman, A. V. Abad, P. Balcombe, P. E. Dodds, P. Ekins, N. Shah, K. R. Ward, Energy Environ. Sci. 2019, 12, 463.
- [6] A. Saeedmanesh, M. A. Mac Kinnon, J. Brouwer, Curr. Opin. Electrochem. 2018, 12, 166.
- [7] Z. Chen, H. Dinh, E. Miller, Photoelectrochemical Water Splitting: Standards, Experimental Methods, and Protocols, Springer-Verlag, New York, 2013.
- [8] O. Legrini, E. Oliveros, A. M. Braun, Chem. Rev. 1993, 93, 671.
- [9] K. C. Christoforidis, P. Fornasiero, ChemCatChem 2017, 9, 1523.
- [10] M. Heinemann, B. Eifert, C. Heiliger, Phys. Rev. B 2013, 87, 115111.
- [11] S. Piccinin, Phys. Chem. Chem. Phys. 2019, 21, 2957.
- [12] A. Walsh, Y. Yan, M. N. Huda, M. M. Al-Jassim, S.-H. Wei, Chem. Mater. 2009, 21, 547.
- [13] C. Wang, H. Qiu, T. Inoue, Q. Yao, Int. J. Hydrogen Energy 2014, 39, 12507.

- [14] S. J. A. Moniz, S. A. Shevlin, D. J. Martin, Z.-X. Guo, J. Tang, Energy Environ. Sci. 2015, 8, 731.
- [15] S. Bai, X. Yang, C. Liu, X. Xiang, R. Luo, J. He, A. Chen, ACS Sustainable Chem. Eng. 2018, 6, 12906.
- [16] K.-H. Ye, H. Li, D. Huang, S. Xiao, W. Qiu, M. Li, Y. Hu, W. Mai, H. Ji, S. Yang, Nat. Commun. 2019, 10, 1.
- [17] L. Zhang, M. Yang, Z. Luo, J. Zhang, Y. Hou, Int. J. Hydrogen Energy 2019. 44. 25652.
- [18] J. Sun, L. Sun, X. Yang, S. Bai, R. Luo, D. Li, A. Chen, Electrochim. Acta **2020**. *331*. 135282.
- [19] T. Zhang, J. Su, L. Guo, CrystEngComm 2016, 18, 8961.
- [20] Y. Pihosh, I. Turkevych, K. Mawatari, J. Uemura, Y. Kazoe, S. Kosar, K. Makita, T. Sugaya, T. Matsui, D. Fujita, M. Tosa, M. Kondo, T. Kitamori, Sci. Rep. 2015, 5, 11141.
- [21] J. Zhang, H. Ma, Z. Liu, Appl. Catal., B 2017, 201, 84.
- [22] W. Wang, M. Xu, X. Xu, W. Zhou, Z. Shao, Angew. Chem., Int. Ed. **2020**, 59, 136.
- [23] S. Y. Chae, C. S. Lee, H. Jung, O.-S. Joo, B. K. Min, J. H. Kim, Y. J. Hwang, ACS Appl. Mater. Interfaces 2017, 9, 19780.
- [24] T. Nakajima, T. Nakamura, T. Tsuchiya, Phys. Chem. Chem. Phys. 2014, 16, 26901.
- [25] B. S. Kalanoor, H. Seo, S. S. Kalanur, Mater. Sci. Energy Technol. 2018, 1, 49.
- [26] J. Zhang, Z. Liu, Z. Liu, ACS Appl. Mater. Interfaces 2016, 8, 9684.
- [27] Y.-S. Chen, L.-Y. Lin, Electrochim. Acta 2018, 285, 164.
- [28] S. Okunaka, Y. Hitomi, H. Tokudome, RSC Adv. 2018, 8, 31575.
- [29] S. Y. Jeong, K. S. Choi, H.-M. Shin, T. L. Kim, J. Song, S. Yoon, H. W. Jang, M.-H. Yoon, C. Jeon, J. Lee, S. Lee, ACS Appl. Mater. Interfaces 2017. 9. 505.
- [30] S. Hilliard, D. Friedrich, S. Kressman, H. Strub, V. Artero, C. Laberty-Robert, ChemPhotoChem 2017, 1, 273.
- [31] Q. Zeng, J. Li, L. Li, J. Bai, L. Xia, B. Zhou, Appl. Catal. B 2017, 217, 21.
- [32] S. M. Thalluri, C. Martinez Suarez, M. Hussain, S. Hernandez, A. Virga, G. Saracco, N. Russo, Ind. Eng. Chem. Res. 2013, 52, 17414.
- [33] X. Ren, Z. Yang, D. Yang, X. Zhang, D. Cui, Y. Liu, Q. Wei, H. Fan, S. (Frank) Liu, Nanoscale 2016, 8, 3816.
- [34] S. Okunaka, Y. Hitomi, H. Tokudome, RSC Adv. 2018, 8, 31575.
- [35] L. Shi, S. Zhuo, M. Abulikemu, G. Mettela, T. Palaniselvam, S. Rasul, B. Tang, B. Yan, N. B. Saleh, P. Wang, RSC Adv. 2018, 8, 29179.
- [36] F. F. Abdi, L. Han, A. H. M. Smets, M. Zeman, B. Dam, R. van de Krol, Nat. Commun. 2013, 4, 2195.
- [37] J. K. Cooper, S. Gul, F. M. Toma, L. Chen, Y.-S. Liu, J. Guo, J. W. Ager, J. Yano, I. D. Sharp, J. Phys. Chem. C 2015, 119, 2969.
- [38] Z. Zhao, Z. Li, Z. Zou, Phys. Chem. Chem. Phys. 2011, 13, 4746.
- [39] P. P. González-Borrero, F. Sato, A. N. Medina, M. L. Baesso, A. C. Bento, G. Baldissera, C. Persson, G. A. Niklasson, C. G. Granqvist, A. Ferreira da Silva, Appl. Phys. Lett. 2010, 96, 061909.
- [40] H. He, S. P. Berglund, A. J. E. Rettie, W. D. Chemelewski, P. Xiao, Y. Zhang, C. B. Mullins, J. Mater. Chem. A 2014, 2, 9371.
- [41] R. Tang, S. Zhou, Z. Yuan, L. Yin, Adv. Funct. Mater. 2017, 27, 1701102.
- [42] X. Wan, F. Niu, J. Su, L. Guo, Phys. Chem. Chem. Phys. 2016, 18,
- [43] C. Zachäus, F. F. Abdi, L. M. Peter, R. van de Krol, Chem. Sci. 2017, 8,
- [44] Y. Huang, Y. Yu, Y. Xin, N. Meng, Y. Yu, B. Zhang, Sci. China Mater. 2017, 60, 193.
- [45] H. He, Y. Zhou, G. Ke, X. Zhong, M. Yang, L. Bian, K. Lv, F. Dong, Electrochim. Acta 2017, 257, 181.
- [46] K. Pingmuang, J. Chen, W. Kangwansupamonkon, G. G. Wallace, S. Phanichphant, A. Nattestad, Sci. Rep. 2017, 7, 8929.



- www.entechnol.de
- [47] F. F. Abdi, N. Firet, R. van de Krol, ChemCatChem 2013, 5, 490.
- [48] B.-C. Xiao, L.-Y. Lin, J.-Y. Hong, H.-S. Lin, Y.-T. Song, RSC Adv. 2017, *7*, 7547.
- [49] C. Martinez Suarez, S. Hernández, N. Russo, Appl. Catal. A 2015, *504*, 158.
- [50] H. W. Jeong, T. H. Jeon, J. S. Jang, W. Choi, H. Park, J. Phys. Chem. C **2013**, *117*, 9104.
- [51] J. H. Seo, G. Park, K. H. Oh, S. H. Kang, H. C. Lee, S. K. Cho, K. M. Nam, J. Electroanal. Chem. 2017, 789, 17.
- [52] L. Xia, J. Bai, J. Li, Q. Zeng, X. Li, B. Zhou, Appl. Catal. B 2016, 183, 224.
- [53] M. G. Lee, D. H. Kim, W. Sohn, C. W. Moon, H. Park, S. Lee, H. W. Jang, Nano Energy 2016, 28, 250.
- [54] S. J. Hong, S. Lee, J. S. Jang, J. S. Lee, Energy Environ. Sci. 2011, *4*, 1781.
- [55] S.-L. Chen, L.-Y. Lin, Y.-S. Chen, Electrochim. Acta 2019, 295, 507.
- [56] E. Warren Bertram, X-Ray Diffraction, Addison-Wesley Pub. Co, Reading, MA 1969.
- [57] T. M. Nahir, J. Am. Chem. Soc. 2005, 127, 12431.